A Bounding Surface Plasticity Model for Unsaturated Structured Soils

H. Moghaddasi, B. Shahbodagh, N. Khalili*

School of Civil and Environmental Engineering, the University of New South Wales, Sydney 2052, Australia.

*Corresponding Author: Nasser Khalili, Professor, School of Civil and Environmental Engineering, the University of New South Wales, Sydney 2052, Australia. Email: n.khalili@unsw.edu.au, Tel: +612-9385-5074.

Abstract:

A bounding surface plasticity model based on the effective stress concept is presented to describe the behaviour of unsaturated structured soils subjected to hydro-mechanical loadings. The structural degradation effects on the compressive and tensile strength are considered through controlling the size of the bounding surface, allowing for a smooth transition of the response from structured to unstructured states. The structural degradation is modelled using a work hardening approach, considering both the effects of stress magnitude and accumulated plastic strain on the degradation process. A void ratio-dependent water retention model is adopted, taking the effect of hydraulic hysteresis into account. Attention is also given to the stiffening effect of a decrease in the degree of saturation on the mechanical response of unsaturated structured soils and the wetting-induced collapse. A radial mapping rule with a mobile centre of homology is adopted to capture the response of the soil under unloading-reloading conditions. The predictive capability of the model is demonstrated through the comparison of the model simulations with experimental data for different conventional laboratory tests including constant-suction oedometer and triaxial shearing and wetting tests.

1. Introduction

Theoretical and experimental investigations of the hydro-mechanical behaviour of geomaterials with initial structure have received much attention amongst geotechnical researchers in the past few decades. Although the definition of structured soils targets only a particular class of geomaterials, such materials often cover a wide range of the shallow strata

This is a peer-reviewed, accepted author manuscript of the following article: Moghaddasi, H., Shahbodagh, B., & Khalili, N. (2021). A bounding surface plasticity model for unsaturated structured soils. Computers and Geotechnics, 138, [104313]. https://doi.org/10.1016/j.compgeo.2021.104313

encountered in civil engineering projects. The hydro-mechanical properties of unsaturated structured soils can be affected by many factors, including water meniscus and initial structure. Due to the presence of initial structure, the material can withstand a relatively high pressure before exhibiting the micro-scale pore structure collapse and strength degradation (Leroueil and Vaughan, 1990). Initial porosity and its evolution with applied stress often provides sufficient information to trace the mechanical behaviour of geomaterials, but it needs to be augmented by structural evaluation if the material reveals a degree of structure (Georgiannou and Burland, 2006). On the other hand, the presence of water in the structured soil can noticeably alter both its hydraulic and mechanical properties. Both changes in degree of saturation and soil structure influence the effective yield pressure, and hence, the hydro-mechanical behaviour of unsaturated structured geomaterials (Leroueil and Barbosa, 2000, Koliji et al., 2009, Arroyo et al., 2013).

During the past two decades, numerous phenomenological constitutive models were developed based on the theory of plasticity for predicting the behaviour of structured soils (Rouainia and Muir Wood, 2000, Kavvadas and Amorosi, 2000, Liu and Carter, 2002, Nova et al., 2003, Baudet and Stallebrass, 2004, Yu et al., 2007, Horpibulsuk et al., 2010, Yan and Li, 2010, Robin et al., 2015, Ouria, 2017). A majority of the models utilise plastic straining to describe changes in the size and the position of the yield surface (Nova et al., 2003, Yan and Li, 2010, Asaoka et al., 2000, Kavvadas and Amorosi, 2000, Rouainia and Muir Wood, 2000, Baudet and Stallebrass, 2004, Yang et al., 2016). However, the simultaneous effects of all plastic strain components, i.e. plastic volumetric and deviatoric strains, have only been considered in some of these models to properly capture destruction process (Nova et al., 2003, Rouainia and Muir Wood, 2000, Yan and Li, 2010). In some of the models, the stress level is considered as a measure for detecting the onset and progression of destruction process (Liu and Carter, 2002, Horpibulsuk et al., 2010, Nguyen et al., 2014). In these models, destruction occurs only when the stress reaches a certain threshold. However, it has been shown that the destructuration of the initial structure occurs due to the simultaneous effects of the stress magnitude and the accumulation of the plastic strain, and that the structural degradation cannot be predicted satisfactorily through the individual effects of stress or strain (Yasin and Tatsuoka, 2000, Xiao et al., 2010). The models were also formulated within the context of the conventional elasto-plastic theory, which is unable to predict destruction and collapse under the stress state below the yield surface. The kinematic hardening models were proposed to capture the behaviour of structured soils under unloading-reloading conditions

(Kavvadas and Amorosi, 2000, Rouainia and Muir Wood, 2000, Baudet and Stallebrass, 2004). However, these models are invariably based on complex hardening rules, with considerable number of model parameters, many of which cannot be determined from standard laboratory tests.

The hydro-mechanical behaviour of unsaturated structured soils is controlled by both the bonded structure and the degree of saturation. Several constitutive models have been developed to capture the essential features of the unsaturated structured soils (Yang et al., 2008, Koliji et al., 2010a, Pereira et al., 2014). Among them, there are a few constitutive models addressing both the effects of partial saturation and structure on the behaviour of the material (Koliji et al., 2010a, Pereira et al., 2014). These models mainly inherit the deficiencies attributed to the conventional constitutive relationships, i.e. an abrupt change from elastic to elastoplastic behaviour and prediction of a purely elastic response due to cycles of loading and unloading. In addition, such models are unable to capture the structure degradation due to mechanical hysteresis, i.e. plastic hysteretic response during cyclic loading, and hydraulic hysteresis. The coupled effects of the hydraulic properties, such as water retention curve and hydraulic conductivity, with the deformation model have not also been addressed in these models. Yang et al. (2008) proposed a bounding surface plasticity model incorporating the combined effects of unsaturation and the initial structure. Although the model aimed at predicting the behaviour of cemented soil under cyclic loading, a fixed projection centre was adopted for the mapping rule which is not suitable for simulating the response of the porous media subject to unloading and reloading cycles. Furthermore, the use of micro-mechanical volumetric parameters for the stiffness and strength degradation makes the calibration of the model difficult if not impossible.

The main objective of this paper is to present a rigorous bounding surface plasticity model for describing the hydro-mechanical behaviour of unsaturated structured soils. The hydraulic characteristics of structured soil are captured through a void ratio-dependent hysteretic water retention model formulated based on the effective stress principle. The effects of structural degradation and the degree of saturation on the compressive and tensile strength of the material are considered through controlling the size of the bounding surface, allowing for a smooth transition of the response from structured to unstructured states. A plastic work hardening approach is adopted to take into account the effects of stress magnitude and accumulated plastic strain on the degradation process. The kinematic hardening is captured through transfer of the centre of homology and the loading surface upon stress reversal. To recover the irreversible collapse behaviour of unsaturated structured soils, a novel incremental elasto-plastic relation is proposed which considers the individual effects of state variables, i.e. matric suction, degree of saturation, strain tensor and net stress. Simulation results and comparisons with experimental test data are presented for a range of saturated and unsaturated structured soils to demonstrate the performance of the model.

2. Preliminaries

To develop the stress-strain relationship, compact matrix-vector notation is adopted with bold face representing matrices and vectors. The plasticity model is expressed in the effective stress space (p'-q-θ), defined as

$$p' = -\frac{\boldsymbol{\sigma}'^{\mathrm{T}}\boldsymbol{\delta}}{3}, \quad q = \sqrt{(3/2)\mathbf{s}^{\mathrm{T}}\mathbf{s}}, \quad \theta = \left(\frac{1}{3}\right)\sin^{-1}\left(-\frac{3\sqrt{3}}{2}\frac{\det[s]}{\sqrt{\left((1/2)\mathbf{s}^{\mathrm{T}}\mathbf{s}\right)^{3}}}\right) \tag{1}$$

where p', q and θ are the mean effective stress, the deviatoric stress and the Lode angle, respectively. $\boldsymbol{\sigma}'$ is the effective stress tensor, $\boldsymbol{\delta}$ is the Kronecker delta and $\mathbf{s}$ is the deviator stress tensors expressed as $\mathbf{s} = \boldsymbol{\sigma}' + p'\boldsymbol{\delta}$. In this definition, the variation of the Lode angle, θ, is between $-\pi/6$ and $+\pi/6$. The volumetric and deviatoric strains are defined as

$$\varepsilon_v = -\boldsymbol{\varepsilon}^{\mathrm{T}}\boldsymbol{\delta}, \quad \varepsilon_q = \frac{2}{\sqrt{3}}\sqrt{(1/2)\mathbf{e}^{\mathrm{T}}\mathbf{e}} \tag{2}$$

in which $\boldsymbol{\varepsilon}$ is the second order strain tensor and $\mathbf{e}$ is the deviator strain tensor given by $\mathbf{e} = \boldsymbol{\varepsilon} + (1/3)\varepsilon_v\boldsymbol{\delta}$. The sign convention of continuum mechanics is used throughout, except for the mean effective stress (p') and the volumetric strain (ε_v) which are defined positive in compression following the soil mechanics convention. The total strain rate is decomposed into the elastic and plastic components

$$\dot{\boldsymbol{\varepsilon}} = \dot{\boldsymbol{\varepsilon}}^{\mathrm{e}} + \dot{\boldsymbol{\varepsilon}}^{\mathrm{p}} \tag{3}$$

where $\dot{\boldsymbol{\varepsilon}}^{\mathrm{e}}$ and $\dot{\boldsymbol{\varepsilon}}^{\mathrm{p}}$ denote the elastic and plastic components of the strain rate, respectively. The relationship between the volumetric strain, ε_v, and the specific volume (υ) is defined as

$$\varepsilon_v = \ln\left(\frac{\upsilon}{\upsilon_0}\right) \tag{4}$$

where υ_0 is the initial specific volume.

3. The effective stress principle and the volume change dependency

Finding a unified methodology for describing the behaviour of saturated and unsaturated soils has long been a subject of great interest in geotechnical engineering. The extension of the effective stress approach for multi-phase porous media has been a significant step in quantitative assessment of the behaviour of unsaturated soils (Kohgo et al., 1993, Khalili and Khabbaz, 1998, Loret and Khalili, 2000, Laloui et al., 2003, Gallipoli et al., 2003, Sheng et al., 2003, Borja, 2004, Alonso et al., 2010, Einav and Liu, 2020). For saturated soils, the effective stress is quantified using Terzaghi's expression (Terzaghi, 1936). The generalised form of the effective stress for unsaturated soils is expressed as (Bishop and Blight, 1963)

$$\boldsymbol{\sigma}' = \boldsymbol{\sigma} + \chi p_w \boldsymbol{\delta} + (1-\chi) p_a \boldsymbol{\delta} = \boldsymbol{\sigma}_{\text{net}} - \chi s \boldsymbol{\delta} \tag{5}$$

where p_w and p_a are the pore water and pore air pressures, respectively, and χ is the effective stress parameter. $s = p_a - p_w$ is the matric suction and $\boldsymbol{\sigma}_{\text{net}} = \boldsymbol{\sigma} + p_a \boldsymbol{\delta}$ is the net stress. The early definition of the effective stress parameter assumed a direct relation with the degree of saturation, which was able to predict the transition between the unsaturated and saturated soils upon wetting. However, the experimental studies did not fully justify the use of the degree of saturation for a wide range of matric suctions. In this model, the effective stress parameter proposed by Khalili and Khabbaz (1998) is adopted

$$\chi = \begin{cases} 1 & s \le s_e \\ \left(\dfrac{s_e}{s}\right)^{\Omega} & s_e < s \le 25 s_e \end{cases} \tag{6}$$

in which χ is defined as *a priori* function of suction. In this equation, s_e is the suction value marking the transition between saturated and unsaturated states. For wetting process, s_e is equal to the air expulsion value, s_{ex}, whereas for drying process, s_e is equal to the air entry value, s_{ae}. Examining the shear strength of unsaturahed soils, it is shown that a constant value of 0.55 can be assumed for Ω (Khalili and Khabbaz, 1998). Notice that the applicability of (6) is limited to $s \le 25 s_e$. Its extension to higher values of suction is provided in Russell and Khalili (2006). The effect of hydraulic hysteresis on the effective stress parameter is captured using the correlation proposed by Khalili et al. (2008) and Khalili and Zargarbashi (2010) for suction reversals:

$$\chi = \begin{cases} \left(\dfrac{s_{ae}}{s_{rd}}\right)^{\Omega} \left(\dfrac{s_{rd}}{s}\right)^{\zeta} & \text{for drying path reversal} \quad \left(\dfrac{s_{ex}}{s_{ae}}\right)^{\Omega/(\Omega\text{-}\zeta)} s_{rd} \le s \le s_{rd} \\ \left(\dfrac{s_{ex}}{s_{rw}}\right)^{\Omega} \left(\dfrac{s_{rw}}{s}\right)^{\zeta} & \text{for wetting path reversal} \quad s_{rw} \le s \le \left(\dfrac{s_{ae}}{s_{ex}}\right)^{\Omega/(\Omega\text{-}\zeta)} s_{rw} \end{cases} \tag{7}$$

where ζ is the slope of the transition line (also referred to as the scanning line) between the main drying and wetting paths in a $\ln(\chi)-\ln(s)$ plane, s_{rd} and s_{rw} are the points of suction reversal on the main drying and main wetting paths, respectively (see Figure 1). Experimental investigations have shown that the air-entry and air-expulsion values are not constant and can markedly change by the volume change of unsaturated soil (Pasha et al., 2017, Raveendiraraj, 2009, Gallipoli et al., 2003). This imposes a strong coupling between the volume change and the water retention curve and the volume change and the effective stress parameter. The rate form of the effective stress equation is obtained through a simple differentiation of Equation (5)

$$\dot{\boldsymbol{\sigma}}' = \dot{\boldsymbol{\sigma}} + \psi \dot{p}_w \boldsymbol{\delta} + (1\text{-}\psi)\dot{p}_a \boldsymbol{\delta} \text{-} \psi_v \dot{\varepsilon}_v \boldsymbol{\delta} = \dot{\boldsymbol{\sigma}}_{\mathrm{net}} \text{-} \psi \dot{s} \boldsymbol{\delta} \text{-} \psi_v \dot{\varepsilon}_v \boldsymbol{\delta} \tag{8}$$

where $\dot{\boldsymbol{\sigma}}'$ is the effective stress rate, $\dot{\varepsilon}_v$ is the volumetric strain rate, $\psi = \partial(\chi s)/\partial s$ is the incremental effective stress parameter, and $\psi_v = \partial(\chi s)/\partial \varepsilon_v$ is the incremental volumetric effective stress parameter which captures the change in the effective stress due to the change in the volumetric strain at constant suction. Notice that the effective stress parameter is *a priori* function of matric suction and the volumetric strain, $\chi(s, \varepsilon_v)$. The dependency of the effective stress parameter to volume change has been schematically depicted in Figure 1.

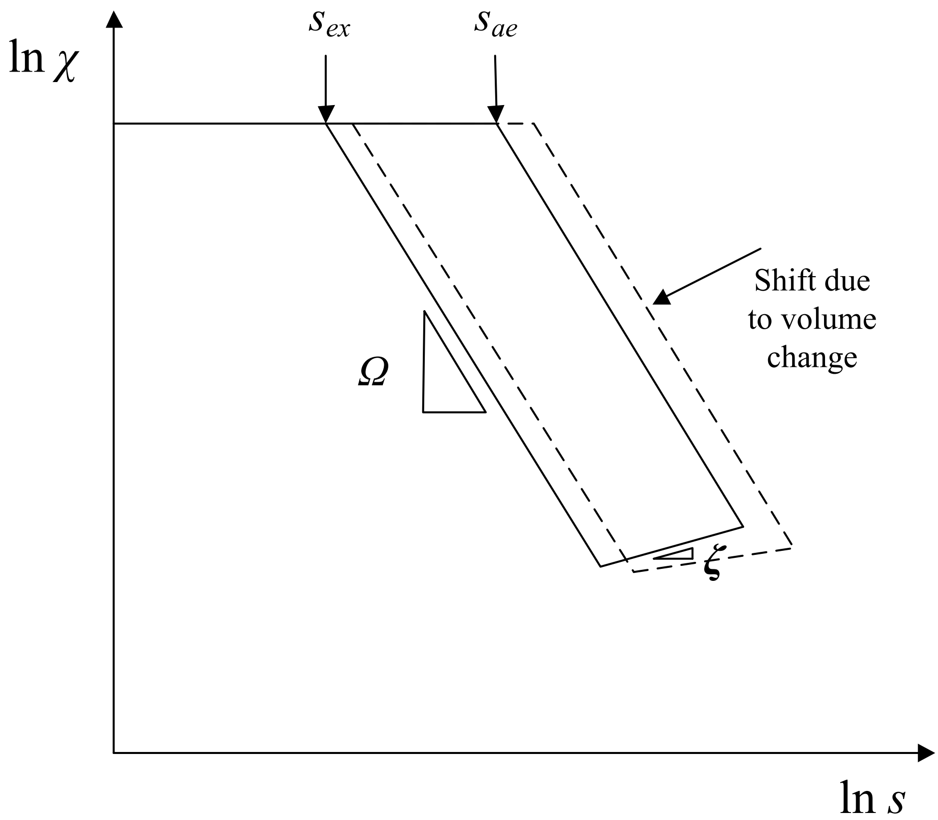

Figure 1: Evolution of the effective stress parameter with hydraulic hysteresis and volume change

4. The void ratio-dependent water retention curve

The soil water retention curve is often expressed as a function of the mass/volumetric water content or the degree of saturation with respect to the matric suction. Numerous models have been proposed in the literature to provide a relationship for the SWRC. The models proposed by Brooks and Corey (1964) and Van Genuchten (1980) are among the popular ones. Due to the simplicity of the expression, the water retention curve proposed by Brooks and Corey (1964) is adopted in the present study,

$$S_{eff} = \begin{cases} 1 & s \le s_e \\ \left(\dfrac{s_e}{s}\right)^{\lambda_p} & s > s_e \end{cases} \tag{9}$$

where λ_p is the pore size distribution index or the slope of WRC in a $\ln(S_{eff}) - \ln(s)$ plane, $S_{eff} = (S_r - S_{res})/(1 - S_{res})$ is the effective degree of saturation, and S_{res} is the residual degree of saturation. To include the effect of hydraulic hysteresis, the equation proposed by Khalili et al. (2008) is used here

$$S_{eff}=\begin{cases}\left(\dfrac{s_{ae}}{s_{rd}}\right)^{\lambda_{pd}}\left(\dfrac{s_{rd}}{s}\right)^{\xi} & \text{for drying path reversal } \dfrac{s_{ex}^{\left(\lambda_{pw}/\left(\lambda_{pw}-\xi\right)\right)}}{s_{ae}^{\left(\lambda_{pd}/\left(\lambda_{pw}-\xi\right)\right)}}s_{rd}^{\left(\left(\lambda_{pd}-\xi\right)/\left(\lambda_{pw}-\xi\right)\right)}\le s\le s_{rd}\\ \left(\dfrac{s_{ex}}{s_{rw}}\right)^{\lambda_{pw}}\left(\dfrac{s_{rw}}{s}\right)^{\xi} & \text{for wetting path reversal } s_{rw}\le s\le \dfrac{s_{ae}^{\left(\lambda_{pd}/\left(\lambda_{pd}-\xi\right)\right)}}{s_{ex}^{\left(\lambda_{pw}/\left(\lambda_{pd}-\xi\right)\right)}}s_{rw}^{\left(\left(\lambda_{pw}-\xi\right)/\left(\lambda_{pd}-\xi\right)\right)}\end{cases}\tag{10}$$

where ξ is the slope of the transition line between the main drying and wetting paths in a $\ln(S_{eff})-\ln(s)$ plane, and λ_{pd} and λ_{pw} are the pore size distribution indexes corresponding to the main drying and wetting curves, see Figure 2. The coupling of the fluid constitutive laws and the effective stress-strain relationship of the soil skeleton can be used to obtain a mathematical expression for the state-dependent water retention curve. The compatibility requirement of the volumetric strain of the three phases is invoked to determine the coupling of the effective stress parameter and the degree of saturation. Utilising the relationship provided by Khalili et al. (2008), the change in the degree of saturation due to volume change can be expressed as

$$dS_r=(\psi-S_r)\frac{de}{e}\tag{11}$$

where e is the void ratio. Based on Eq. (11), the updated degree of saturation due to the evolution of the void ratio for any given value of suction can be written for the main drying or wetting curves as (Pasha et al., 2017)

$$S_{eff}^{*}=S_{eff}+dS_{eff}=\left(\frac{s_e}{s}\right)^{\lambda_p}+\frac{\left[(1-\Omega)\left(\dfrac{s_e}{s}\right)^{\Omega}-(1-S_{res})\left(\dfrac{s_e}{s}\right)^{\lambda_p}-S_{res}\right]de}{e(1-S_{res})}\tag{12}$$

In order to calculate the updated air-entry/air-expulsion value (s_e^{*}), Eq. (12) can be examined at its limit of transition from saturation to unsaturation, where $S_{eff}^{*}=1$ and $s=s_e^{*}$,

$$\frac{(1-\Omega)de}{e(1-S_{res})}\left(\frac{s_e}{s_e^*}\right)^{\Omega}+(1-\frac{de}{e})\left(\frac{s_e}{s_e^*}\right)^{\lambda_{psu}}-\left[1+\frac{S_{res}de}{e(1-S_{res})}\right]=0 \tag{13}$$

in which λ_{psu} is the pore size distribution index at s_e^*. Using Taylor's series expansion of Eq. (13), a simplified expression can be obtained for the updated air-entry/air-expulsion value with void ratio as (Pasha et al., 2017, Moghaddasi et al., 2017)

$$s_e^* = s_e\left[1+\frac{\Omega}{(1-S_{res})}\frac{de}{e}\right]^{-1/\lambda_{psu}} \tag{14}$$

This can be further simplified if the small changes in void ratio is applied (Mašín, 2010)

$$s_e^* = s_e\left[1-\frac{\Omega}{(1-S_{res})\lambda_{psu}}\frac{de}{e}\right] \tag{15}$$

The chain rule can be employed to capture the dependency of λ_p to the void ratio

$$\frac{\partial S_r}{\partial e}=\frac{\partial S_r}{\partial s_e}\frac{\partial s_e}{\partial e}+\frac{\partial S_r}{\partial \lambda_p}\frac{\partial \lambda_p}{\partial e} \tag{16}$$

The variation of the pore size distribution index with respect to the void ratio can be obtained by substituting Eqs. (15), (11) and (9) into Eq. (16)

$$\frac{\partial \lambda_p}{\partial e}=\frac{\left(\psi-S_r+\Omega S_{eff}\dfrac{\lambda_p}{\lambda_{psu}}\right)\lambda_p}{e(1-S_{res})S_{eff}\ln(S_{eff})} \tag{17}$$

It is clear from Eq. (17) that there is some dependency of $\partial\lambda_p/\partial e$ to matric suction. Such dependency is, however, very slight (see Pasha et al., 2017) and can be eliminated if Eq. (17) is linearised between points $(s_e/s=1, S_{eff}=1)$ and $(s_e/s=(1/2)^{1/\lambda_p}, S_{eff}=1/2)$. This results in a suction independent expression for the updated pore size distribution index

$$\lambda_p^* = \lambda_p\left\{1-\frac{3\left[(1-\Omega)(2^{(1-\Omega/\lambda_p)}-1)-S_{res}\right]}{2(1-S_{res})}\frac{de}{e}\right\} \tag{18}$$

If the hydraulic state is located on the scanning curve, the updated effective degree of saturation can be obtained, in a similar manner to Eq. (12), as

$$S_{eff}^{*}=S_{eff}+dS_{eff}=\left(\frac{s_e}{s_r}\right)^{\lambda_p}\left(\frac{s_r}{s}\right)^{\xi}+\frac{\left[(1-\zeta)\left(\frac{s_e}{s_r}\right)^{\Omega}\left(\frac{s_r}{s}\right)^{\zeta}-(1-S_{res})\left(\frac{s_e}{s_r}\right)^{\lambda_p}\left(\frac{s_r}{s}\right)^{\xi}-S_{res}\right]de}{e(1-S_{res})} \tag{19}$$

where $s_r = s_{rd}$ refers to the suction at the point of reversal from the main drying path, and $s_r = s_{rw}$ represents the suction at the point of reversal from the main wetting path. Using the Taylor's series expansion of Eq. (19), the updated slope of the scanning curve (ξ^*) at $s = s_r$ is derived as

$$\xi^{*}=\xi\left\{1+\frac{(1-\zeta)(\zeta-\xi)}{\xi}\left(\frac{s_e}{s_r}\right)^{\Omega-\lambda_p}\frac{de}{e}\right\} \tag{20}$$

The updated hydraulic parameters of the model are shown in Figure 2.

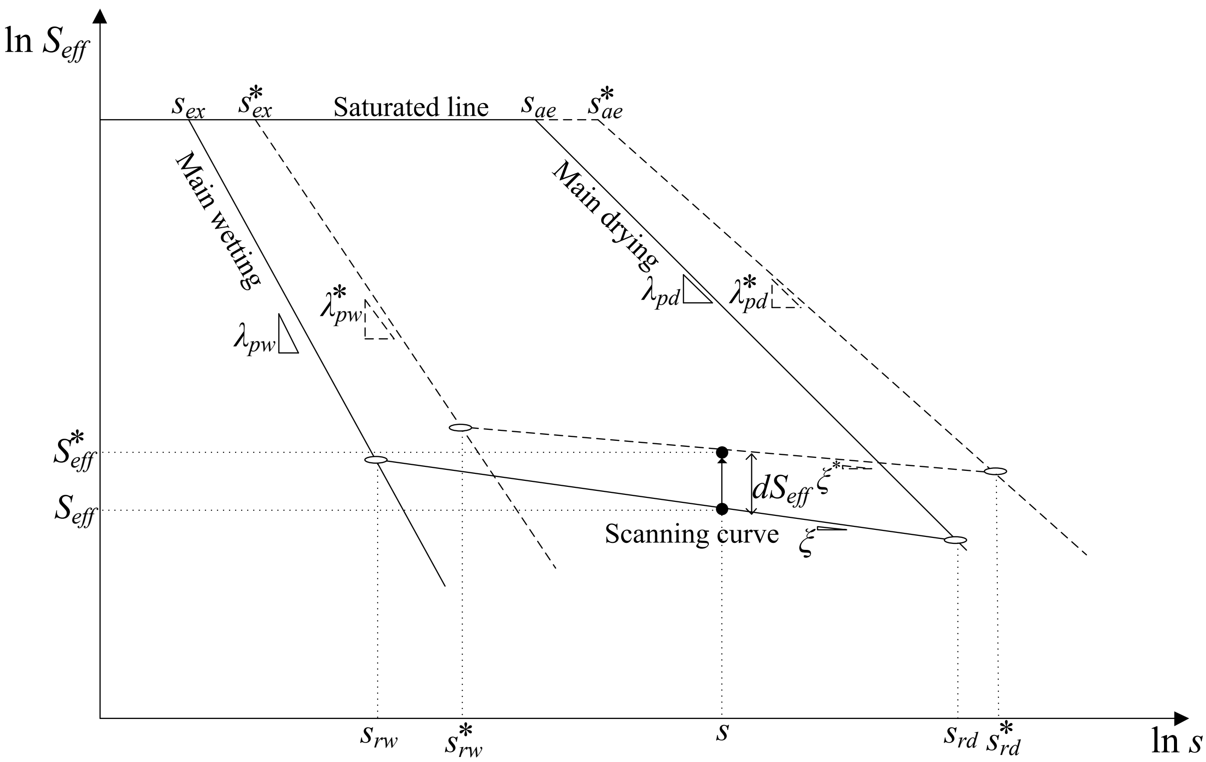

Figure 2: The evolution of the main drying, wetting and scanning curves due to the volume change

5. Critical state and limiting isotropic lines

There is an ultimate state for soil towards which all stress states approach with increasing deviatoric shear strain (Wood, 1990, Russell and Khalili, 2004). This is referred to as the "critical state" and can be assumed a straight line in the $\upsilon - \ln p'$ plane. Similar behaviour is also observed in structured soils when initial structure is broken due to accumulation of deviatoric shear strain (Wesley, 1990, Amorosi and Rampello, 2007). For unsaturated soils, the critical state condition depends not only on the mechanical loading but also on the hydraulic state of the material and the value of matric suction (Wheeler and Sivakumar, 1995, Loret and Khalili, 2002, Russell and Khalili, 2006). Both influences can be effectively captured by rendering CSL a function of the degree of saturation, S_r, rather than suction, s. To fulfil this condition, the following line representation is used for the CSL

$$\upsilon_{cs} = \Gamma(S_r) - \lambda(S_r)\ln(p'_{cs} / p'_1) \tag{21}$$

where p'_{cs} and υ_{cs} are the mean effective stress and specific volume at the critical state, respectively, $\Gamma(S_r)$ is the specific volume on the CSL at the reference pressure p'_1 (typically taken unity) and $\lambda(S_r)$ is the slope of the CSL in the $\upsilon - \ln p'$ plane (see Figure 3). The proximity of the current state relative to the CSL in the $\upsilon - \ln p'$ plane can be measured and expressed in terms of a state dependent dimensionless parameter

$$\xi_{cs} = \upsilon - \upsilon_{cs}(p') \tag{22}$$

in which υ is the specific volume at the current stress state and $\upsilon_{cs}(p')$ is the specific volume at the critical state corresponding to the current stress. The state parameter quantifies the relative density of the unstructured material with respect to that at the critical state. The CSL can be represented in the $p' - q$ plane by a straight line passing through the origin. The slope of the CSL, M_{cs}, in the general stress space can be linked to the Lode angle through (Sheng et al., 2000; Khalili et al., 2008)

$$M_{cs}(\theta) = M_{max}\left[\frac{2\alpha^4}{1+\alpha^4 - \left(1-\alpha^4\right)\sin\left(3\theta\right)}\right]^{1/4} \tag{23}$$

in which $\alpha = M_{min} / M_{max}$ with M_{max} and M_{min} being the slope of the CSL at triaxial compression and extension, respectively. M_{max} and M_{min} can be linked to the critical state friction angle

$$M_{max} = \frac{6\sin\left(\phi'_{cs}\right)}{3-\sin\left(\phi'_{cs}\right)} \tag{24}$$

$$M_{min} = \frac{6\sin\left(\phi'_{cs}\right)}{3+\sin\left(\phi'_{cs}\right)} \tag{25}$$

in which ϕ'_{cs} is the critical-state internal frictional angle. To define the hardening modulus, the behaviour of the material subjected to isotropic compression needs to be obtained. For a geomaterial, this is typically captured through existence of a limiting isotropic compression line (LICL) defined as a reference line parallel to the CSL with a constant shift in the $\upsilon - \ln p'$ plane along the recompression line. For unstructured soils, the LICL is the limit of all admissible states of stress and represents the loosest possible state of a soil at a given mean effective stress. The presence of initial structure leads to the excess compressive strength of the soil and a shift to the right of the LICL. In Figure 3, the shift in the LICL due to strength of structure is denoted by $\bar{p}'_m$ and the shift in the LICL due to change in the degree of saturation is denoted by $\bar{p}'_s$. For the reconstituted material, the specific volume on the LICL in the presence of suction is represented by

$$\upsilon_{LICL} = N(S_r) - \lambda(S_r)\ln(\bar{p}'_s / p'_1) \tag{26}$$

where $N(S_r)$ is the intercept of the LICL at the reference pressure p'_1, and υ_{LICL} is the specific volume on the LICL. $N(S_r)$ is related to $\Gamma(S_r)$ by

$$N(S_r) = \Gamma(S_r) + \left(\lambda\left(S_r\right) - \kappa\right)\ln(R) \tag{27}$$

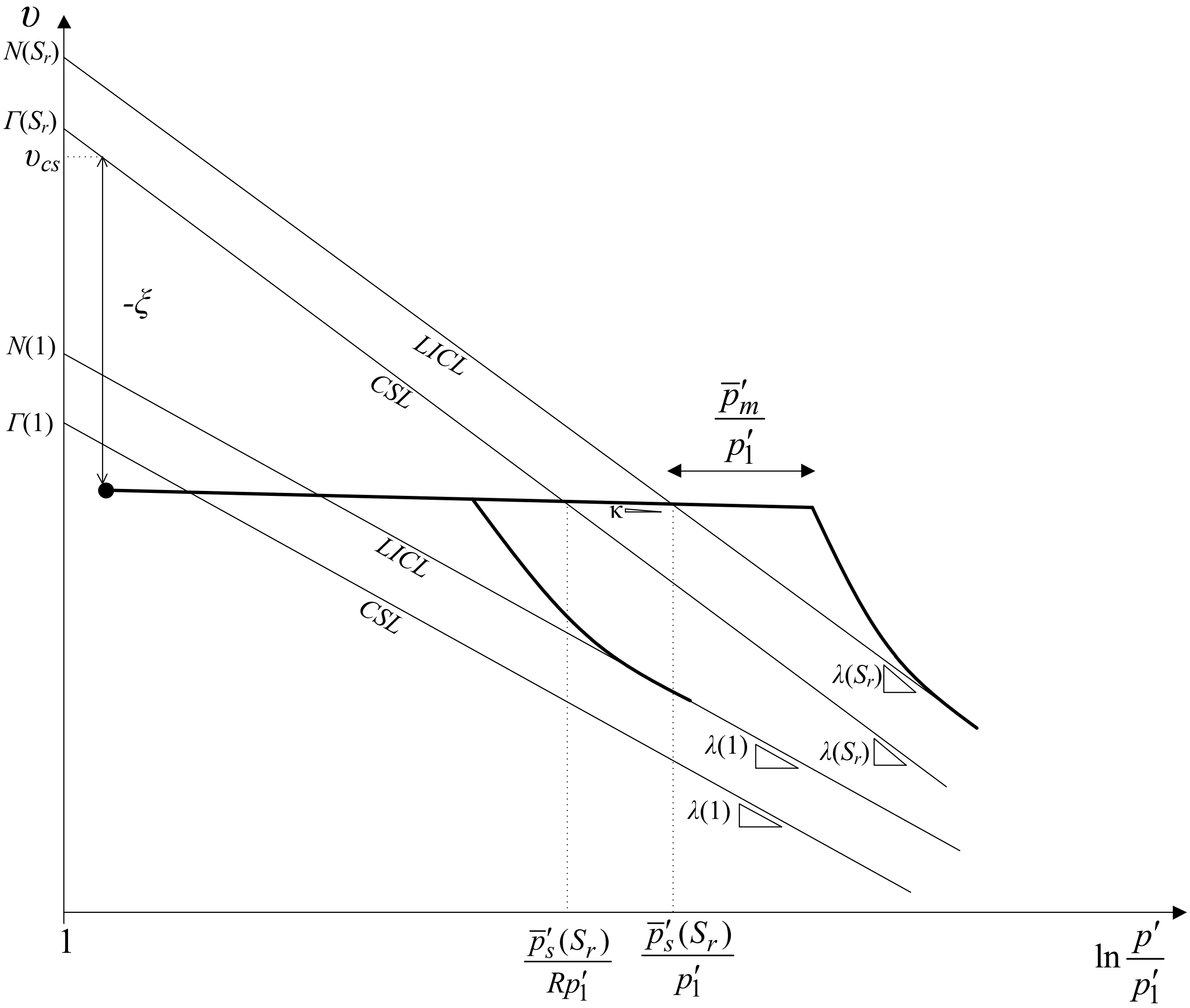

Figure 3: The critical state and limiting isotropic lines for unsaturated structured soils

in which R is the model parameter representing the distance between the CSL from the LICL along the κ line in the $\upsilon - \ln p'$ plane. Following the coupled approach proposed by Loret and Khalili (2002), the stiffening effects on $\bar{p}'_s$ due to a decrease in the degree of saturation and an increase in the plastic volumetric strain can be expressed as

$$\bar{p}'_s\left(\varepsilon_v^p, S_r\right) = \bar{p}'_{s0}\Pi\left(S_r\right)\exp\left(\frac{\upsilon_i \Delta\varepsilon_p^p}{\lambda\left(S_r\right) - \kappa}\right) \tag{28}$$

where

$$\Pi\left(S_r\right) = \exp\left(\frac{N\left(S_r\right) - N\left(1\right)}{\left(\lambda\left(S_r\right) - k\right)} - \frac{\lambda\left(S_r\right) - \lambda\left(1\right)}{\lambda\left(1\right) - k}\ln\left(\frac{\bar{p}'_{s0}}{p'_1}\right)\right) \tag{29}$$

υ_i is the initial specific volume, $\bar{p}'_{s0}$ is the initial value of the hardening parameter $\bar{p}'_s$ at the fully saturated state, and $\Delta\varepsilon_p^p$ is the increment of the plastic volumetric strain. Also, $N(1)$ and $\lambda(1)$ are the intercept and the slope of the LICL at the fully saturated state. In this formulation, the additive effect of the degree of saturation and initial structure is assumed in the absence of sufficient experimental studies justifying the multiplicative effects. A graphical representation of the LICL and CSL in the $\upsilon - \ln p'$ is shown in Figure 3.

6. Elastic behaviour

The elastic component of the strain rate tensor is linked to the effective stress rate tensor through,

$$\dot{\boldsymbol{\sigma}}' = \mathbf{D}^{\mathrm{e}} \dot{\boldsymbol{\varepsilon}}^{\mathrm{e}} \tag{30}$$

in which $\mathbf{D}^{\mathrm{e}}$ is the elastic property matrix, defined as

$$\mathbf{D}^{\mathrm{e}} = \begin{bmatrix} K & 0 \\ 0 & 3G \end{bmatrix} \tag{31}$$

where K and G are the bulk and shear moduli, respectively. The moduli can be assumed to be constant in certain confining pressures for the highly structured soils. However, for the slightly structured soils, the bulk and shear moduli depend a priori on the confining pressure. The moduli can then be defined as

$$K = \frac{\upsilon p'}{\kappa} \tag{32}$$

$$G = \frac{3(1-2\nu)}{2(1+\nu)} \frac{\upsilon p'}{\kappa} \tag{33}$$

where ν is the Poisson's ratio.

7. Bounding surface

The bounding surface is the limit of admissible states of stress within the material. The shape of the bounding surface can be determined from the undrained response of the material in its loosest state, where the contribution of elasticity to volume change is negligible. Following the work of (Khalili et al., 2005), the bounding surface for structured soils can be defined as (see Figure 4)

$$F(\bar{p}'^{*},\bar{q},\bar{\theta},\bar{p}'_c)=\left(\frac{\bar{q}}{M_{cs}\left(\bar{\theta}\right)\bar{p}'^{*}}\right)^{N}-\frac{\ln\left(\bar{p}'_c/\bar{p}'^{*}\right)}{\ln R}=0 \tag{34}$$

where

$$\begin{aligned}\bar{p}'_c&=\bar{p}'_t+\bar{p}'_s+\bar{p}'_m\\ \bar{p}'^{*}&=\bar{p}'+\bar{p}'_t\end{aligned} \tag{35}$$

$\bar{p}'_t$ and $\bar{p}'_m$ are the isotropic tensile strength and the increase in the isotropic pre-consolidation pressure due to the structure, and $\bar{p}'_s$ is the isotropic reconsolidation pressure at fully destructed state. N and R are the material parameters controlling the shape of the bounding surface (Yu, 1998). The material constant R represents the ratio between $\bar{p}'_c$ and the value of $\bar{p}'^{*}$ at the intercept of the bounding surface with the CSL in the stress space. The curvature of the bounding surface is controlled by the parameter N. The superimposed bar denotes stress conditions on the bounding surface.

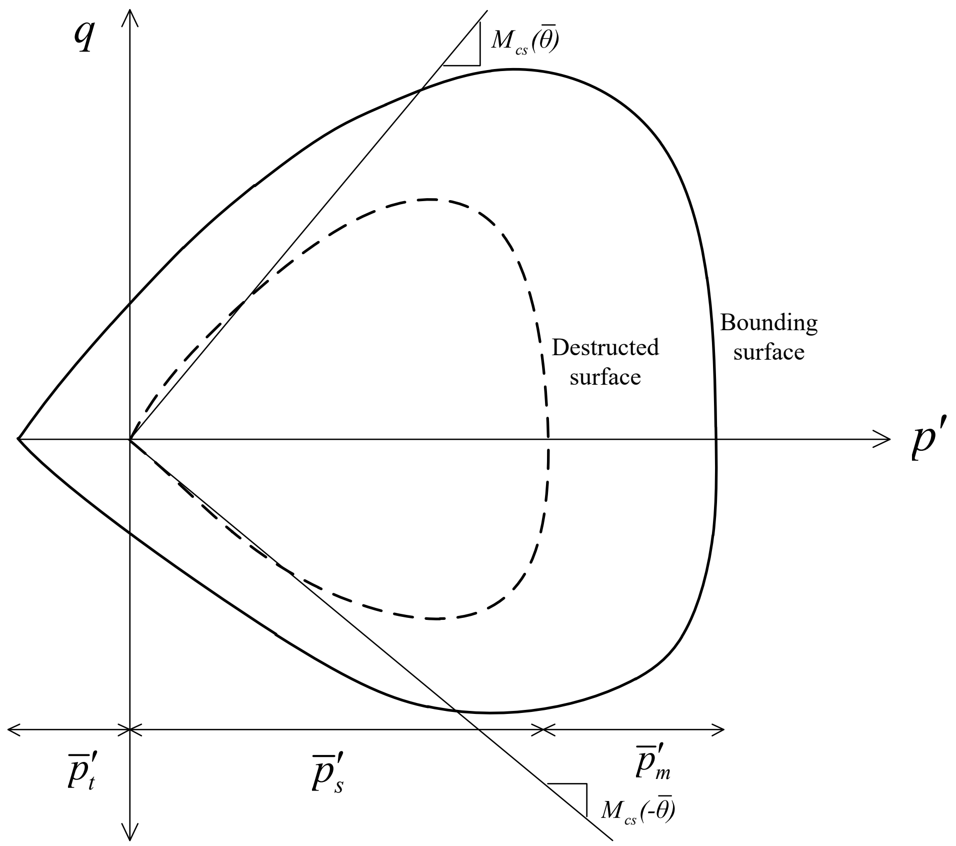

Figure 4: The shape of bounding surface for structured soils in the $p'-q$ plane.

The experimental studies on structured soils revealed that the strength degradation can occur by increasing applied shear stress and progress until structure is destroyed in the material (Nguyen et al., 2014, Georgiannou and Burland, 2006, Leroueil and Vaughan, 1990). The frictional contacts between grains carry the major part of the load when the structural effect decreases substantially. By destructuration of structure due to shearing, the state of stress can move towards the critical state line, where no volumetric strain occurs (Yan and Li, 2010). This behaviour of the structured soil can be captured through controlling the model parameters, $\overline{p}'_m$, $\overline{p}'_t$ and $\overline{p}'_s$. The shrinkage of the bounding surface due to the structural degradation is captured via $\overline{p}'_m$ and $\overline{p}'_t$, while the hardening/softening behaviour of the soil after the destruction phase is controlled though the evolution of $\overline{p}'_s$ with plastic volumetric strain and the degree of saturation. At large strains, the values of $\overline{p}'_m$ and $\overline{p}'_t$ approach zero and the bounding surface is reduced to that for reconstituted fully destructed material.

8. Loading surface and mapping rule

The equivalency of the unit vector normal to the loading surface at $\boldsymbol{\sigma}'$ with the unit vector normal to the bounding surface at $\bar{\boldsymbol{\sigma}}'$ requires the similarity of shapes between the two surfaces. The loading surface is assumed to be homologous to the bounding surface about the centre of homology as

$$f\left(\hat{p}'^{*}, \hat{q}, \hat{\theta}, \hat{p}'_c\right)=\left[\frac{\hat{q}}{M_{cs}\left(\hat{\theta}\right).\hat{p}'^{*}}\right]^{N}-\frac{\ln\left(\hat{p}'_c/\hat{p}'^{*}\right)}{\ln\left(R\right)}=0 \tag{36}$$

where

$$\hat{p}'^{*}=p'^{*}-p'_{\alpha},\ \hat{q}=q-q_{\alpha},\ \hat{\theta}=\theta-\theta_{\alpha},\ \hat{p}'_c=p'_c-p'_{\alpha},\ \boldsymbol{\alpha}=\left\{p'_{\alpha},q_{\alpha},\theta_{\alpha}\right\} \tag{37}$$

$\hat{p}'_c$ controls the size of the loading surface and $\boldsymbol{\alpha}$ is the kinematic hardening vector defining the location of the loading surface. An image point on the bounding surface can be identified by using a mapping rule. The radial mapping rule is used in this study for finding the image point on the bounding surface, which is mathematically expressed as (Moghaddasi et al., 2021)

$$\bar{\boldsymbol{\sigma}}'(\beta)=\left(\boldsymbol{\sigma}'-\boldsymbol{\sigma}'_{\mathrm{H}}\right)\beta+\boldsymbol{\sigma}'_{\mathrm{H}} \tag{38}$$

where $\boldsymbol{\sigma}'$, $\boldsymbol{\sigma}'_{\mathrm{H}}$ and $\bar{\boldsymbol{\sigma}}'(\beta)$ are the current stress point, the stress at the centre of homology and the image point, respectively. β is a scalar value which is obtained by substituting the image stress into the bounding surface equation. From the similarity of the bounding and loading surfaces, the origin of the loading surface, $\boldsymbol{\sigma}'_{\alpha}$, can be calculated as

$$\boldsymbol{\sigma}'_{\alpha}=\left(\frac{\beta-1}{\beta}\right)\boldsymbol{\sigma}'_{\mathrm{H}} \tag{39}$$

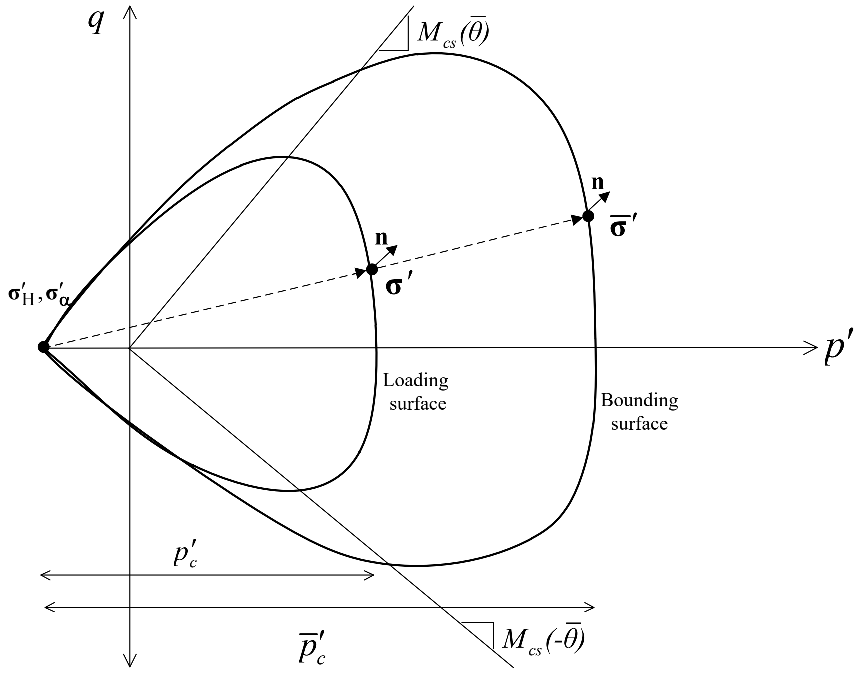

Figure 5: Bounding surface, loading surface and mapping rule for first time loading

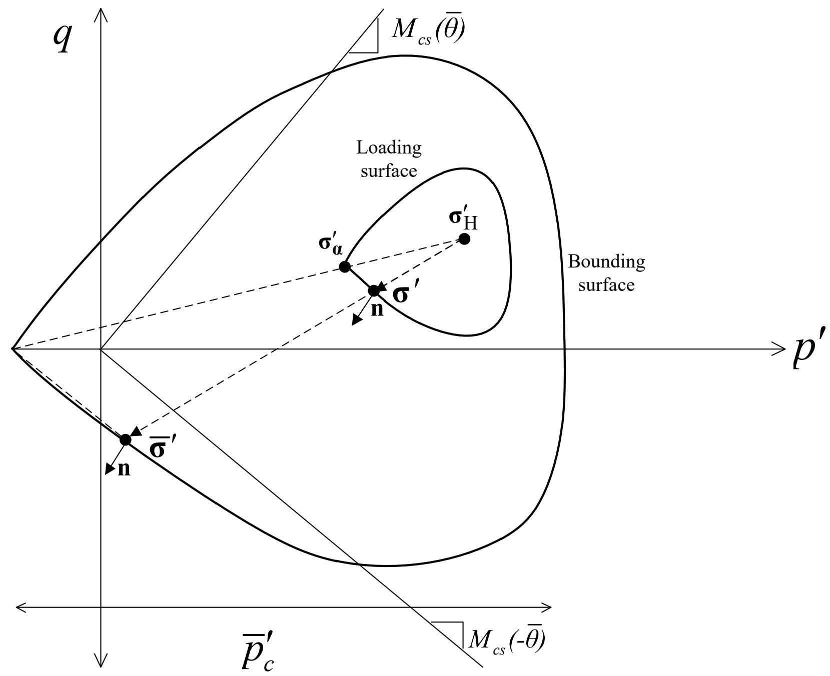

Figure 6: Bounding surface, loading surface and mapping rule during unloading/reloading stage

In the conventional bounding surface plasticity framework, the origin of stress coordinate system is typically used as a centre of homology. However, this is not suitable for the analysis of geomaterials under cyclic loading (Khalili et al., 2005, Hu and Liu, 2015, Shahbodagh et al., 2017, Shahbodagh et al., 2020). In this work, the stress point corresponding to the isotropic tensile strength of the material is selected as the centre of homology for first time loading (see Figure 5), while the last point of stress reversal is used as the centre of homology for the subsequent loading cycles (see Figure 6). The point of stress reversal is detected when the product of the unit vector of loading $\mathbf{n}$ and the "elastic stress" increment ($\dot{\boldsymbol{\sigma}}'_{\mathrm{e}} = \mathbf{D}^{\mathrm{e}}\dot{\boldsymbol{\varepsilon}}$) becomes negative. The unit normal vector at the image point controlling the direction of loading is given by $\mathbf{n} = \dfrac{\partial F / \partial \bar{\boldsymbol{\sigma}}'}{\left\| \partial F / \partial \bar{\boldsymbol{\sigma}}' \right\|} = \dfrac{\partial f / \partial \boldsymbol{\sigma}'}{\left\| \partial f / \partial \boldsymbol{\sigma}' \right\|}$.

9. Plastic potential

The direction of the plastic strain increment can be obtained from the normal to the plastic potential at the current stress point. The relationship between the plastic dilatancy $d\left(= \dot{\varepsilon}_p^p / \dot{\varepsilon}_q^p\right)$ and the stress increment is regarded as the flow rule which is often quantified experimentally. Alternatively, the energy dissipated during plastic deformation can be used to establish the dilatancy law. The total plastic work may be obtained from

$$\dot{W}^p = \boldsymbol{\sigma}'\dot{\boldsymbol{\varepsilon}}^{\mathrm{p}} = p'\dot{\varepsilon}_p^p + q\dot{\varepsilon}_q^p \tag{40}$$

For soils with initial structure, it can be assumed that the dissipation of energy stored between grains is due to both frictional mechanism and the destructuration of initial structure. A generalised form of the energy dissipation equation proposed by Rowe (1962) can be employed for the structured soils to take into account the effect of structure

$$\dot{E}^p = M_f (p' + \bar{p}'_t)\dot{\varepsilon}_q^p - \bar{p}'_t \dot{\varepsilon}_p^p \tag{41}$$

where M_f is a material parameter controlling the amount of energy dissipation. The equality of internal and external energy can be written as

$$p'\dot{\varepsilon}_p^p + q\dot{\varepsilon}_q^p = M_f (p' + \bar{p}'_t)\dot{\varepsilon}_q^p - \bar{p}'_t \dot{\varepsilon}_p^p \tag{42}$$

Rearranging the above equation results in

$$d=\frac{\dot{\varepsilon}_p^p}{\dot{\varepsilon}_q^p}=\left(M_f-\frac{q}{p'^*}\right) \tag{43}$$

To include both the Lode angle dependency of the CSL and the stress path dependency on the dilatancy law, a generalised form of the above equation can be expressed as

$$d=\frac{\dot{\varepsilon}_p^p}{\dot{\varepsilon}_q^p}=A\left(M_{cs}\left(\theta\right)-\tilde{t}\,\frac{q}{p'^*}\right) \tag{44}$$

where A is a material parameter and $\tilde{t}$ is a loading direction multiplier, which quantifies the stress path dependency of dilatancy law. If A is set to zero, no plastic volumetric strain would be obtained. Using A=2 yields an expression similar to the dilatancy law used in the modified Cam clay model, and if A=1 is used, the original Rowe's dilatancy is recovered. By integrating the dilatancy law with respect to the stress, the plastic potential function is obtained as

$$\begin{aligned} g(p'^*,q,\theta,p'_0)&=\tilde{t}q+M_{cs}\left(\theta\right)p'^*\ln\left(p'^*/p'_0\right) \text{ for } A=0 \\ g(p'^*,q,\theta,p'_0)&=\tilde{t}q+\frac{AM_{cs}\left(\theta\right)p'^*}{A-1}\left(\left(\frac{p'^*}{p'_0}\right)^{A-1}-1\right)\text{for } A\neq 0 \end{aligned} \tag{45}$$

where p'_0 is a dummy variable controlling the size of the plastic potential. $\tilde{t}$ is a scalar which indicates the direction of the plastic flow (Khalili et al., 2005). The relative position of the stress point $\boldsymbol{\sigma}'$ and the image point $\bar{\boldsymbol{\sigma}}'$ controls the value of parameter $\tilde{t}$ as

$$\tilde{t}=+1 \ \text{ for}\left|\gamma_{\bar{\sigma}}\text{ - }\gamma_{\sigma}\right|<\pi/2 \quad , \qquad \tilde{t}=-1 \ \text{ for}\left|\gamma_{\bar{\sigma}}\text{ - }\gamma_{\sigma}\right|>\pi/2 \tag{46}$$

where γ_{σ} and $\gamma_{\bar{\sigma}}$ are the angles from a given reference axis to the stress point and the image point, respectively. The shape of the plastic potential surface in the $p'-q$ plane is depicted in Figure 7.

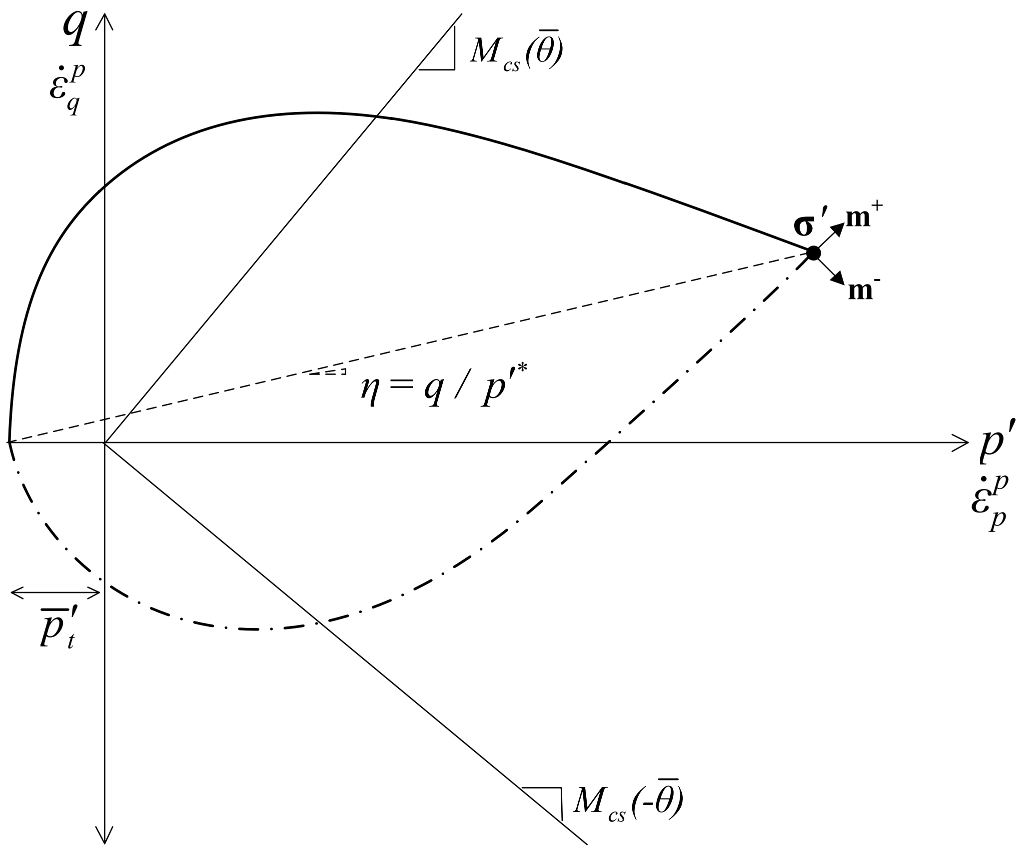

Figure 7: The shape of the plastic potential in the stress space for compression and extension loadings.

The direction of the plastic flow is determined as

$$\mathbf{m} = \frac{\partial g / \partial \boldsymbol{\sigma}'}{\left\| \partial g / \partial \boldsymbol{\sigma}' \right\|} \tag{47}$$

10. Hardening modulus

The hardening modulus in the bounding surface plasticity consists of two terms

$$h = h_b + h_f \tag{48}$$

where h is the hardening modulus at the current stress state $\boldsymbol{\sigma}'$, h_b is the hardening modulus at the image point $\bar{\boldsymbol{\sigma}}'$ on the bounding surface, and h_f is an arbitrary modulus defined as a decreasing function of the distance between the current stress and the image point on the bounding surface. h_b is obtained by applying the consistency condition to the bounding surface. The consistency condition for unsaturated structured soils is written as

$$\dot{F}\left(\bar{\boldsymbol{\sigma}}', \bar{p}_t'(I_s), \bar{p}_m'(I_s), \bar{p}_s'\left(\varepsilon_p^p, S_r\right)\right) = \left(\frac{\partial F}{\partial \bar{\boldsymbol{\sigma}}'}\right)^T \dot{\bar{\boldsymbol{\sigma}}}' + \frac{\partial F}{\partial \bar{p}_t'}\frac{\partial \bar{p}_t'}{\partial I_s}\dot{I}_s + \frac{\partial F}{\partial \bar{p}_m'}\frac{\partial \bar{p}_m'}{\partial I_s}\dot{I}_s + \frac{\partial F}{\partial \bar{p}_s'}\frac{\partial \bar{p}_s'}{\partial \varepsilon_p^p}\dot{\varepsilon}_p^p + \frac{\partial F}{\partial \bar{p}_s'}\frac{\partial \bar{p}_s'}{\partial S_r}\dot{S}_r = 0 \tag{49}$$

In the above equation, the change in the size of the bounding surface is linked to the plastic volumetric strain, the degree of saturation and the structure index (I_s). The latter index is introduced to account for the effect of structure on the deformation response of the soil. It is assumed that both compression and tensile responses are influenced by the structure index, i.e. $\bar{p}_m'(I_s)$ and $\bar{p}_t'(I_s)$, while the effects of the saturation degree and the plastic volumetric strain on the bounding surface is captured by $\bar{p}_s'(\varepsilon_p^p, S_r)$. The structure index can be determined following the work hardening approach as

$$\dot{I}_s = \rho_c(1 - I_s)(\dot{w}^p / p_1') \tag{50}$$

where ρ_c is the material parameter quantifying the rate of structure degradation and $\dot{w}^p$ is the absolute rate of plastic work defined as $\dot{w}^p = \left|p'\dot{\varepsilon}_p^p\right| + \left|q\dot{\varepsilon}_q^p\right|$. The integration of Eq. (50) with respect to the plastic work results in an explicit relationship for the structure index. It can be shown that I_s is zero for undisturbed material, while this index approaches one for a completely destructured material. The following relationships are assumed for the change of internal variables, $\bar{p}_m'(I_s)$ and $\bar{p}_t'(I_s)$, with respect to the plastic structure index

$$\frac{\partial \bar{p}_m'}{\partial I_s} = \frac{-\bar{p}_m'}{(1 - I_s)} \quad , \quad \frac{\partial \bar{p}_t'}{\partial I_s} = \frac{-\bar{p}_t'}{(1 - I_s)} \tag{51}$$

As discussed in the previous section, the response of destructured material can be assumed to lay on a straight line in the $\upsilon - \ln p'$ plane. To achieve this behaviour in the model, the following hardening law is adopted

$$\frac{\partial \bar{p}_s'}{\partial \varepsilon_p^p} = \frac{\upsilon \bar{p}_s'}{\lambda(S_r) - \kappa} \tag{52}$$

The plastic volumetric and deviatoric strains are obtained by using the flow rule

$$\dot{\varepsilon}_p^p = \dot{\Lambda} m_p, \quad \dot{\varepsilon}_q^p = \dot{\Lambda} m_q \tag{53}$$

where $\dot{\Lambda}$ is the plastic multiplier and

$$m_p = \frac{\partial g / \partial p'^*}{\left\| \partial g / \partial \boldsymbol{\sigma}' \right\|}, \quad m_q = \frac{\partial g / \partial q}{\left\| \partial g / \partial \boldsymbol{\sigma}' \right\|} \tag{54}$$

The consistency condition can be rewritten using the unit normal vector at the bounding surface

$$\dot{F} = \mathbf{n}^{\mathbf{T}} \dot{\bar{\boldsymbol{\sigma}}}' - \dot{\Lambda} h_b + \frac{\partial F}{\partial \bar{p}'_c} \frac{\partial \bar{p}'_c}{\partial S_r} \dot{S}_r \Big/ \left\| \frac{\partial F}{\partial \bar{\boldsymbol{\sigma}}'} \right\| = 0 \tag{55}$$

Noting that $\dot{w}^p = \dot{\Lambda}\left(\left| p' m_p \right| + \left| q m_q \right| \right)$ and $\frac{\partial \bar{p}'_c}{\partial I_s} = \frac{\partial \bar{p}'_m}{\partial I_s} + \frac{\partial \bar{p}'_t}{\partial I_s}$, h_b can be determined by using Eqs. (50) to (55)

$$h_b = h_t + h_s + h_m \tag{56}$$

where

$$h_t = \frac{1}{\left\| \partial F / \partial \bar{\boldsymbol{\sigma}}' \right\|} \frac{\partial F}{\partial \bar{p}'_t} \left(\frac{\rho_c \bar{p}'_t}{p'_1} \left(\left| p' m_p \right| + \left| q m_q \right| \right) \right) \tag{57}$$

$$h_s = -\frac{1}{\left\| \partial F / \partial \bar{\boldsymbol{\sigma}}' \right\|} \frac{\partial F}{\partial \bar{p}'_s} \left(\frac{\upsilon \bar{p}'_s}{\lambda(S_r) - \kappa} m_p \right) \tag{58}$$

$$h_m = \frac{1}{\left\| \partial F / \partial \bar{\boldsymbol{\sigma}}' \right\|} \frac{\partial F}{\partial \bar{p}'_m} \left(\frac{\rho_c \bar{p}'_m}{p'_1} \left(\left| p' m_p \right| + \left| q m_q \right| \right) \right) \tag{59}$$

The hardening modulus h_f is defined such that it is zero on the bounding surface and infinity at the centre of homology. The following analytical function is proposed for h_f

$$h_f = \frac{\upsilon p'^*}{\left(\lambda(S_r) - \kappa \right)} \left[\frac{\bar{p}'_c}{\hat{p}'_c} - 1 \right] k_m (\eta_p - \tilde{t} \eta) \tag{60}$$

where $\eta = q / p'^*$ is the stress ratio, $\eta_p = \tilde{t}\left(1 - k \xi_{cs}\right) M_{cs}(\theta) \frac{\bar{p}'_c}{\bar{p}'_s}$ is the slope of the peak strength line, k is a material parameter, and k_m is a scaling parameter controlling the hardening modulus. The value of k_m can be different for the first time loading (k_{mf}) and for the subsequent unloading/reloading (k_{mu}).

11. Elastoplastic stress-strain relationship

The equivalent form of the consistency condition at the current stress point $\boldsymbol{\sigma}'$ can be expressed as

$$\mathbf{n}^{\mathbf{T}}\dot{\boldsymbol{\sigma}}' - \dot{\Lambda}h + \frac{\partial F}{\partial \bar{p}'_c}\frac{\partial \bar{p}'_c}{\partial S_r}\dot{S}_r \Big/ \left\|\frac{\partial F}{\partial \bar{\boldsymbol{\sigma}}'}\right\| = 0 \tag{61}$$

Based on this equation, the plastic multiplier is obtained as

$$\dot{\Lambda} = \frac{\mathbf{n}^{\mathbf{T}}\dot{\boldsymbol{\sigma}}' + \frac{\partial F}{\partial \bar{p}'_c}\frac{\partial \bar{p}'_c}{\partial S_r}\dot{S}_r \Big/ \left\|\frac{\partial F}{\partial \bar{\boldsymbol{\sigma}}'}\right\|}{h} \tag{62}$$

The plastic strain rate is derived from a non-associated flow rule and will be given by

$$\dot{\boldsymbol{\varepsilon}}^p = \dot{\Lambda}\mathbf{m} \tag{63}$$

To build the incremental stress-strain relationship, Eq. (3) can be re-written as

$$\dot{\boldsymbol{\sigma}}' = \mathbf{D}^{\mathrm{e}}\dot{\boldsymbol{\varepsilon}}^{\mathrm{e}} = \mathbf{D}^{\mathrm{e}}(\dot{\boldsymbol{\varepsilon}} - \dot{\Lambda}\mathbf{m}) \tag{64}$$

Now combining Eqs. (64) and (62) yields,

$$\dot{\Lambda} = \frac{\mathbf{n}^{\mathbf{T}}\mathbf{D}^{\mathrm{e}}\dot{\boldsymbol{\varepsilon}} + \frac{\partial F}{\partial \bar{p}'_c}\frac{\partial \bar{p}'_c}{\partial S_r}\dot{S}_r \Big/ \left\|\frac{\partial F}{\partial \bar{\boldsymbol{\sigma}}'}\right\|}{h + \mathbf{n}^{\mathbf{T}}\mathbf{D}^{\mathrm{e}}\mathbf{m}} \tag{65}$$

Substituting the expression obtained for the plastic multiplier into Eq. (64) yields

$$\dot{\boldsymbol{\sigma}}' = \left[\mathbf{D}^{\mathrm{e}} - \frac{\mathbf{D}^{\mathrm{e}}\mathbf{m}\mathbf{n}^{\mathbf{T}}\mathbf{D}^{\mathrm{e}}}{h + \mathbf{n}^{\mathbf{T}}\mathbf{D}^{\mathrm{e}}\mathbf{m}}\right]\dot{\boldsymbol{\varepsilon}} - \frac{\mathbf{D}^{\mathrm{e}}\mathbf{m}\frac{\partial F}{\partial \bar{p}'_c}\frac{\partial \bar{p}'_c}{\partial S_r}\dot{S}_r \Big/ \left\|\frac{\partial F}{\partial \bar{\boldsymbol{\sigma}}'}\right\|}{h + \mathbf{n}^{\mathbf{T}}\mathbf{D}^{\mathrm{e}}\mathbf{m}} = \mathbf{D}^{\mathrm{ep}}\dot{\boldsymbol{\varepsilon}} + \mathbf{D}_{\mathrm{s}}^{\mathrm{ep}}\dot{S}_r \tag{66}$$

in which the second term on the right-hand side captures the evolution of the bounding surface due to the change in the degree of saturation. Decomposing the plasticity into stress driven and S_r-hardening/softening components enables capturing wetting-induced collapse in unsaturated soils in a numerically robust manner.

12. Parameter identification

The elastic parameters κ and ν can be specified from the standard triaxial or isotropic compression tests. κ is the initial slope of the isotropic unloading/reloading line in the $\upsilon \sim \ln p'$ plane. Poisson's ratio ν can be identified from the shear modules determined from the initial slope of the volumetric strain vs the deviatoric strain curve. M_{max} is the slope of the critical state line in the $p'-q$ plane. The asymptotic response of the material under large shear strain generating no volume change can be used for the determination of this parameter. Parameters N and R can be identified by fitting the shape of the bounding surface to the experimental data. By plotting the dilatancy ratio with respect to the stress ratio, the material parameter A can be obtained.

Material parameters related to the presence of structure (ρ_c and $\bar{p}'_m$) can be obtained by conducting isotropic compression tests under zero suction and interpreting the data. Under this test, the material parameters $\Gamma(1)$ and $\lambda(1)$ can be found by fitting a tangent line to the destructed state of the compression curve. Empirical relationships can be used to relate $\bar{p}'_t$ to unconfined compressive strength test data. The critical state parameters for unsaturated soil $\Gamma(S_r)$ and $\lambda(S_r)$ can be obtained through conducting a series of isotropic compression tests on unsaturated samples at constant water content. Finally, the model requires a number of material parameters to specify the reference water retention curve. The initial value for the air-entry (s_{ae0}) and the pore size distribution index (λ_{pd0}) can be determined through drying test performed under constant void ratio condition (e_0). Similarly, the material parameters related to the main wetting curve can be selected from the conventional wetting tests (i.e., s_{ex0} and λ_{pw0}). The initial slope of the scanning curve ξ_0 is found by fitting WRC of a drying or wetting path.

13. Application of the model to simulating the behaviour of partially saturated unstructured soils

Experimental tests on Pearl clay

In this section, a number of experimental tests on Pearl clay under combined hydro-mechanical loading are simulated. Sun et al. (2007) investigated the effects of initial void ratio on the water retention and mechanical behaviour of unsaturated Pearl clay samples. The model parameters are calibrated from the experimental data reported by Sun et al. (2007). Mechanical properties and degree saturation dependent hardening parameters of the soil are given in Table 1 and 2. The soil water retention curves (SWRCs) for Pearl clay are shown in Figure 8. The parameters extracted from SWRC are listed in Table 3, obtained from straight line fits to the main drying, main wetting, and scanning experimental data as shown in the Figure 8. Mechanical parameters have been obtained from the saturated and unsaturated isotropic compression responses (e.g. $\lambda(1)$, $\lambda(S_r)$, $\Gamma(S_r)$,$\Gamma(1)$), as shown in Figure 9. A linear interpolation/extrapolation law has been followed to determine the variation of LICL parameters (e.g. $\lambda(1)$, $\lambda(S_r)$, $\Gamma(S_r)$,$\Gamma(1)$) with respect to the degree of saturation. Deviatoric test results are used to obtain critical state and dilatancy parameters (e.g. A and M_{max}). The void ratio dependent air-entry/air-expulsion values using the void ratio dependent WRC model are in turn utilized to determine the contribution of suction to the mean effective stress.

Table 1. The mechanical properties of the soils

Soil	κ	ν	M_{max}	N	R	A	k_{mf}	k_{mu}	k	$\bar{p}'_m$ *(kPa)*	$\bar{p}'_t$ *(kPa)*	ρ_c
Pearl clay	0.03	0.1	1.15	2	1.9	1.3	5	5	2	0	0	0
Natural aggregated soils	0.02	0.4	1.27	2	1.5	2	2	20	2	130	0	0.002

Table 2. Degree saturation dependent properties of the soils

	Pearl clay			Natural aggregated soils				
S_r	1	0.59	0.48	1	0.261	0.199	0.170	0.133
$\lambda(S_r)$	0.12	0.19	0.3	0.06	0.21	0.22	0.22	0.23
$\Gamma(S_r)$	2.689	3.143	3.858	1.833	2.992	3.133	3.223	3.403

Table 3. Water retention properties of the soils

Soil	e_0	s_{ae0} (kPa)	s_{ex0} (kPa)	λ_{pd0}	λ_{pw0}	ξ_0
Pearl clay	1.3	45	10	0.35	0.28	0.15
Natural aggregated soils	0.48	300	-	0.25	-	-

The results from four samples of Pearl clay with different initial void ratios, compressed isotopically from the mean net stress of 20 kPa at a constant at 147 kPa, were simulated numerically based on the proposed plasticity model. The results are presented in Figure 10. It can be seen that the model proposed predicts the behaviour of unsaturated Pearl clay under compression load, and accurately estimates the variation of the degree of saturation due to the change in the soil density.

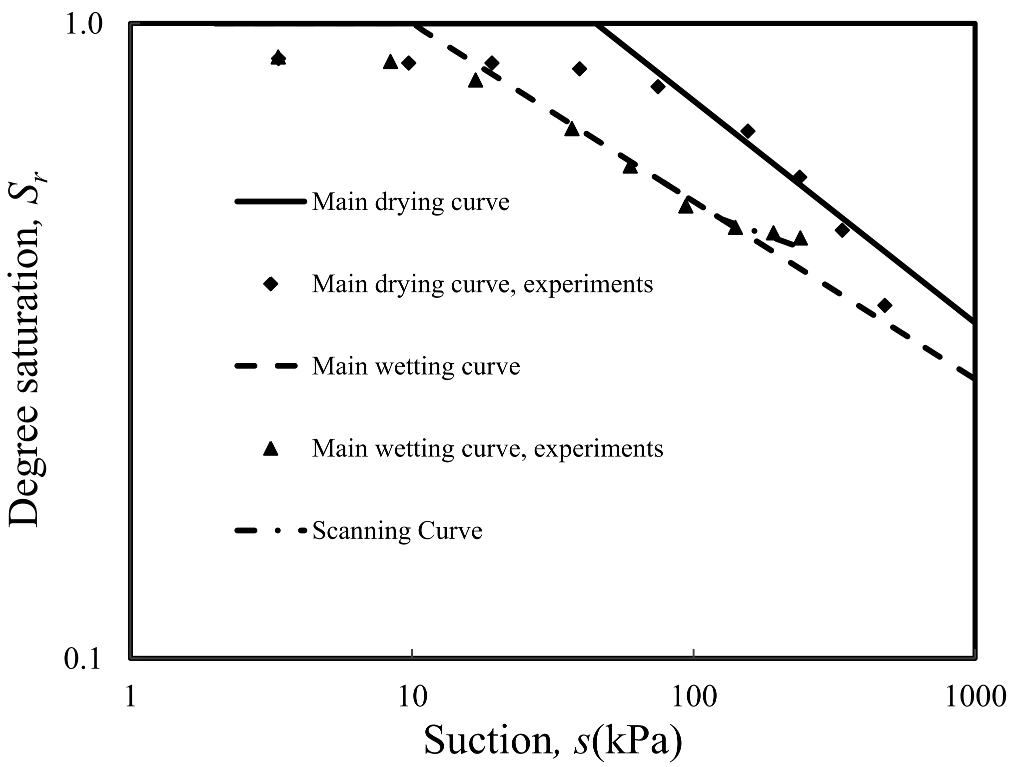

Figure 8: Water retention curves for Pearl clay ($e_0 = 1.26$ is for drying curve, and $e_0 = 1.2$ is for wetting test)

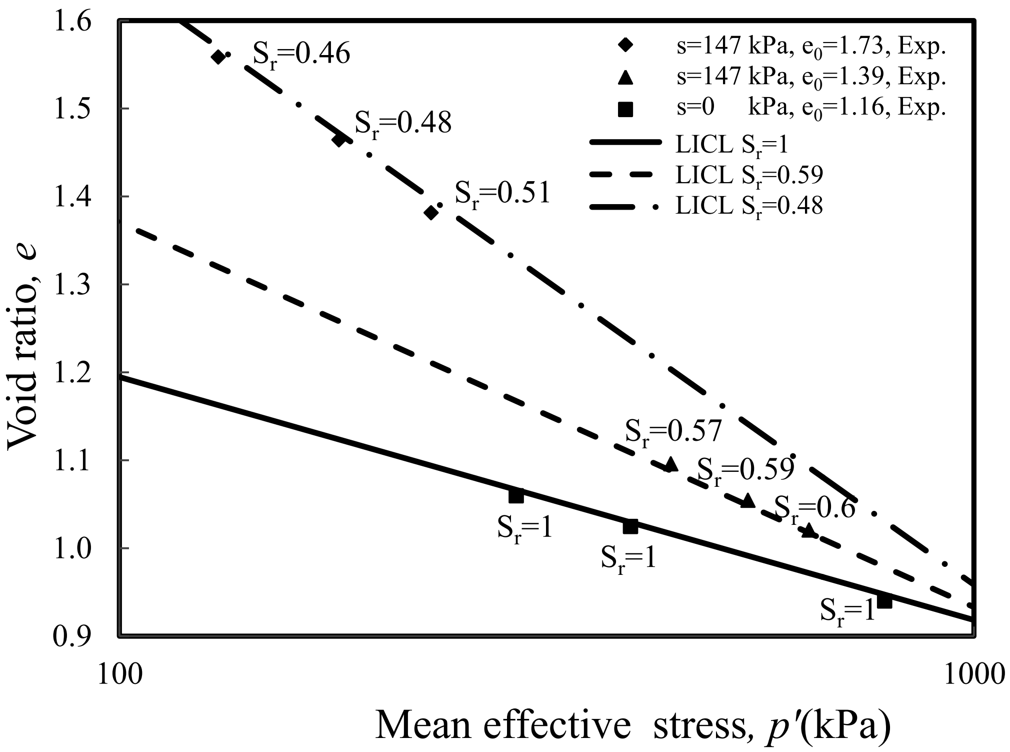

Figure 9: Determination of LICL parameters from isotropic compression tests

Also numerically simulated were two isotropic compression tests performed at constant suction of 147 kPa. The samples were prepared at almost the same void ratio and were compressed to mean net stresses of 196 kPa and 390 kPa, followed by a wetting test. The results of this hydro-mechanical analysis in terms of the change in the void ratio and the degree of saturation are shown in Figure 11. Figure 11a shows that the void ratio in both samples decreases gradually by increasing the cell pressure up to the onset of the wetting test where a sudden reduction in the void ratio is noted due to the collapse of samples. This behaviour is well captured in the numerical simulation. The predicted and measured values for the change of the degree of saturation with respect to matric suction are depicted in Figure 11b. The model predicts satisfactorily the changes in the degree of saturation recorded during the first stage of loading and the subsequent noticeable increase in the degree of saturation observed during the wetting. As the hysteresis in the water retention curve is incorporated into the model, the transition from scanning to main wetting is noted in the numerical simulation. Retention curve is very important but not its small twists and turns. The retention model adopted captures adequately the points of air entry and air expulsion and the slopes of desaturation and wetting lines.

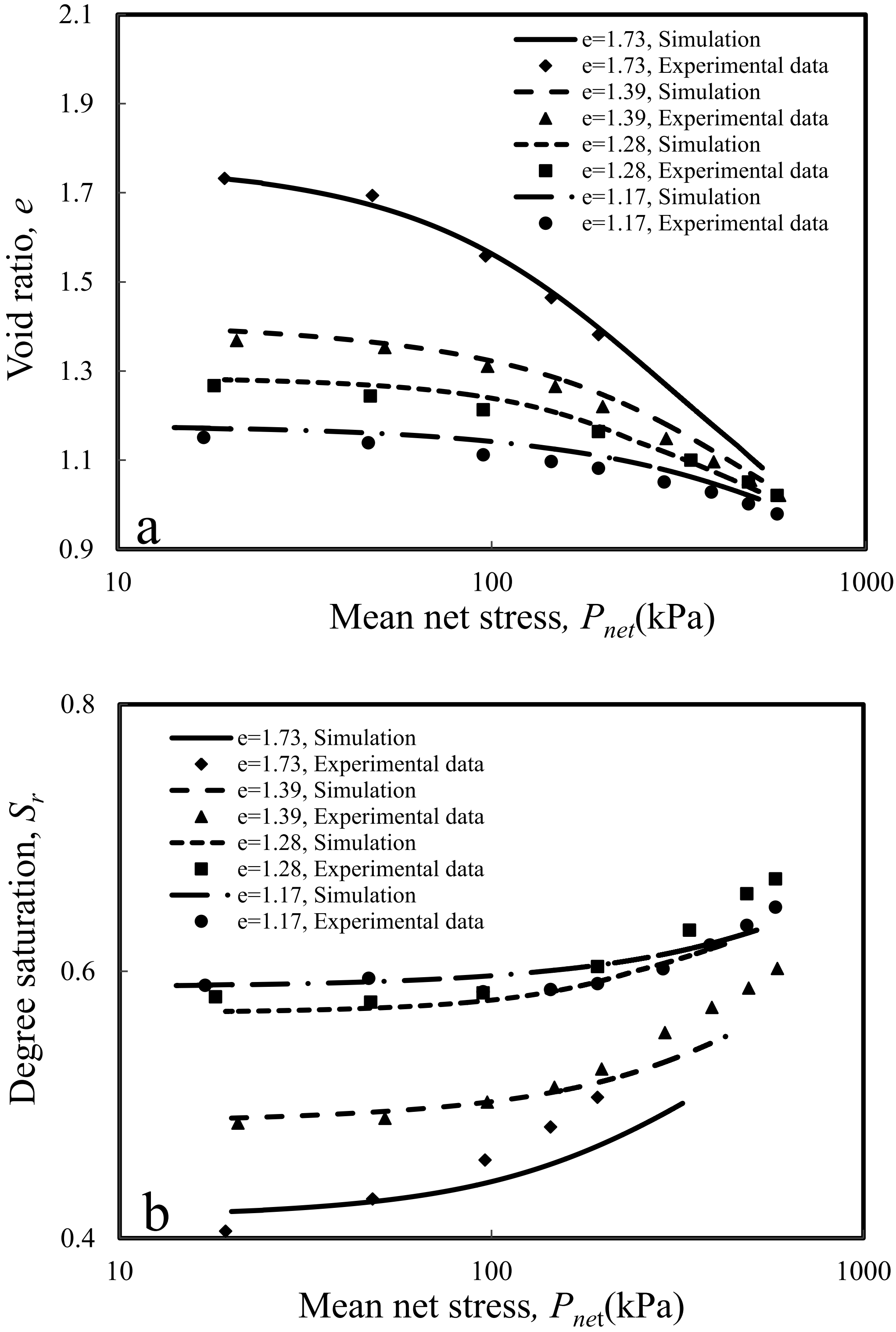

Figure 10: Simulation of isotropic compression test under constant suction = 147 kPa: a) void ratio vs. mean net stress b) degree of saturation vs. mean net stress.

To demonstrate the performance of the model under deviatoric loading, including hydraulic wetting, the combined hydro-mechanical loading path test conducted by Sun et al. (2007) is analysed. Two samples of unsaturated Pearl clay with different initial densities were subjected to a constant suction of 147 kPa and then sheared (at constant suction) until the net stress ratio of σ_1 / σ_3=2 was reached. Subsequently, both samples were soaked to zero suction, followed by shearing to failure. The simulation results and comparison with experimental data are illustrated in Figures 12 and 13 for the initial void ratios of 1.27 and 1.35, respectively. Good agreement is observed between the experimental and numerical simulation results. During the wetting phase of the compacted sample (e_0=1.27), a slight initial swelling followed by a noticeable collapse was observed. This was due to the over-consolidated nature of the soil, with the initial stress state of the sample located within the bounding surface. For the loose sample (e_0=1.35), wetting induced swelling was absent from the response and the reduction of suction entirely resulted in the collapse shrinkage of the sample.

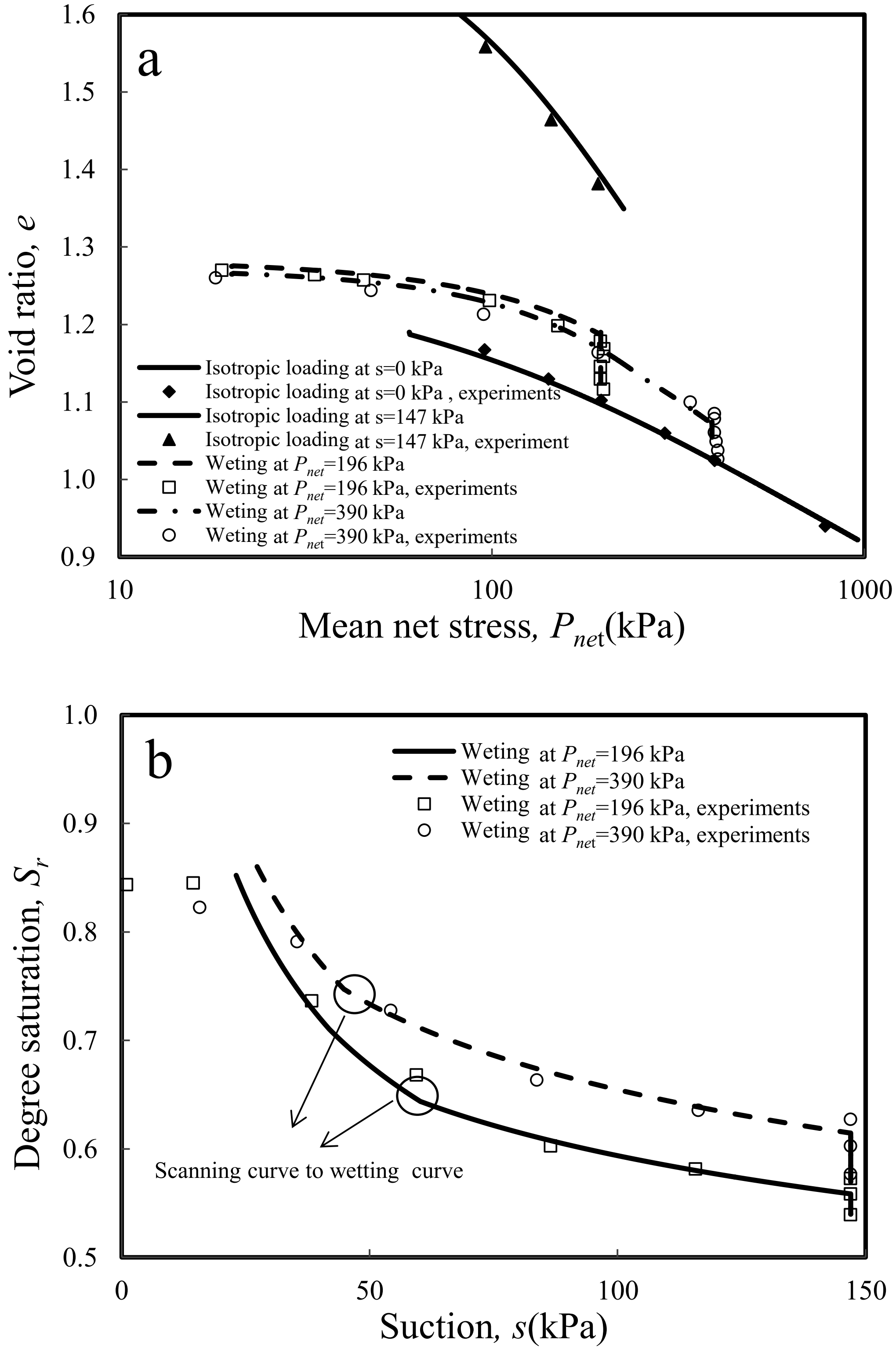

Figure 11: Simulation of isotropic constant water content compression test followed by wetting test: a) void ratio vs. mean net stress, b) the degree of saturation vs. matric suction

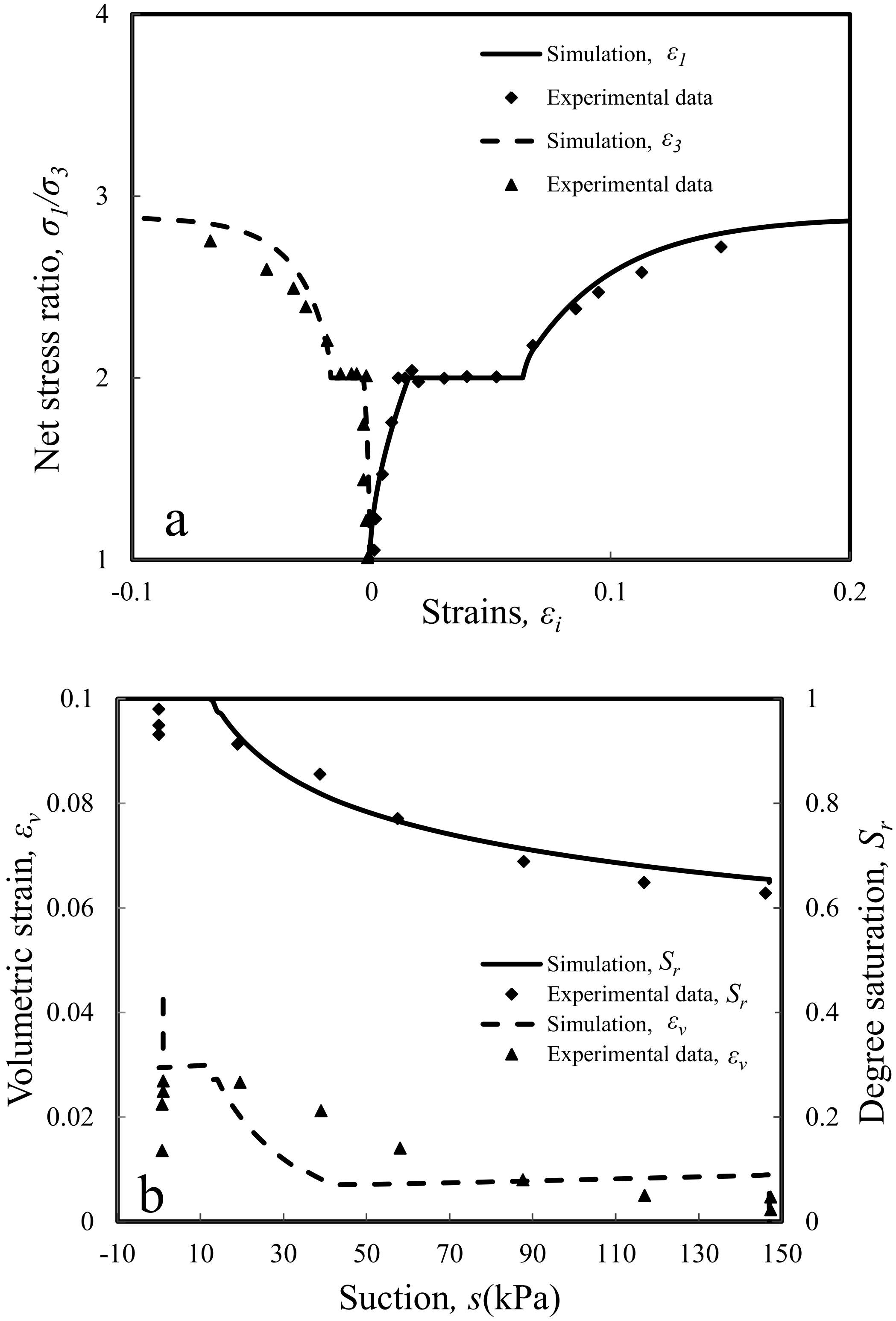

Figure 12: Simulation of triaxial compression and wetting tests for $e_0 = 1.27$: a) net stress ratio vs. strains b) the degree of saturation and the volumetric strain vs. matric suction

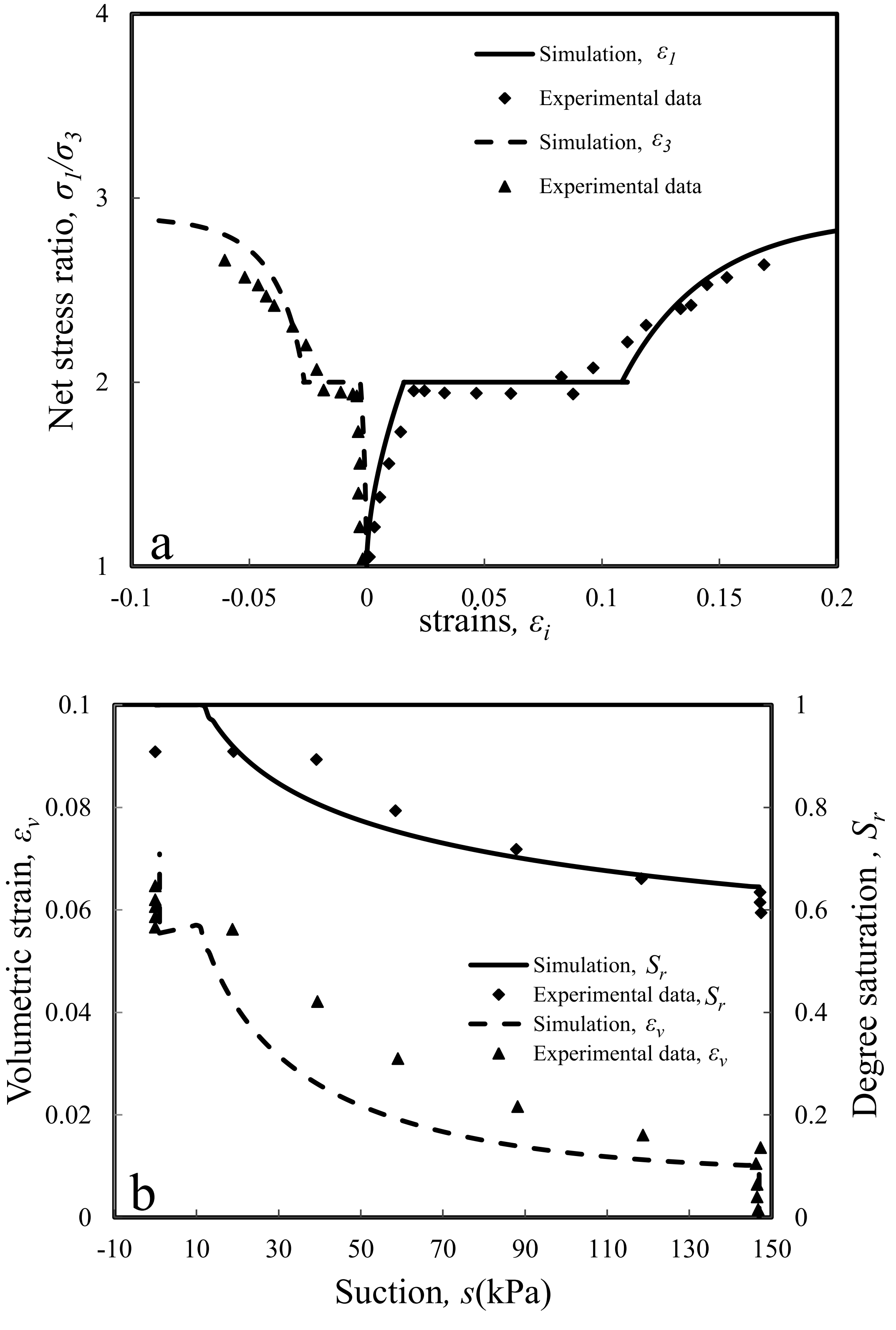

Figure 13: Simulation of the triaxial compression and wetting test for $e_0 = 1.35$: a) net stress ratio vs. strains b) the degree of saturation and the volumetric strain vs. matric suction

14. Application of the model in simulating the behaviour of partially saturated structured soils

Experimental tests on unsaturated aggregated soil

Koliji et al. (2009)(2010b) conducted a series of suction-controlled oedometer tests on natural aggregated soils to explore the combined effects of suction and initial structure. The aggregated soils are primarily composed of clay particles binding the granular materials creating the soil structure. The aggregates were characterised as having high porosity and permeability. The laboratory tests were performed on this soil at both reconstituted and aggregated conditions. The osmotic oedometer system was to apply the target suction. To determine the basic saturated model parameters, the response of saturated reconstituted soil under oedometric conditions test was analysed (Koliji et al., 2010b). The material parameters obtained are summarised in the Table 1.

The water retention properties of the reconstituted soil were investigated in a suction controlled oedometer. After initial saturation and consolidation of the sample to the vertical net stress of 15 kPa, the sample was subjected to drying at constant net stress through increasing suction from zero to 3000 kPa in discrete steps. The test was then followed by performing an oedometer compression test at constant suction value. Figure 14 depicts the measured degree of saturation versus suction obtained from this test. The corresponding model parameters are listed in Table 3. The degree of saturation dependent critical state parameters (Table 2) were determined through the analysis of the constant suction deviatoric and oedometer tests on aggregated unsaturated soils.

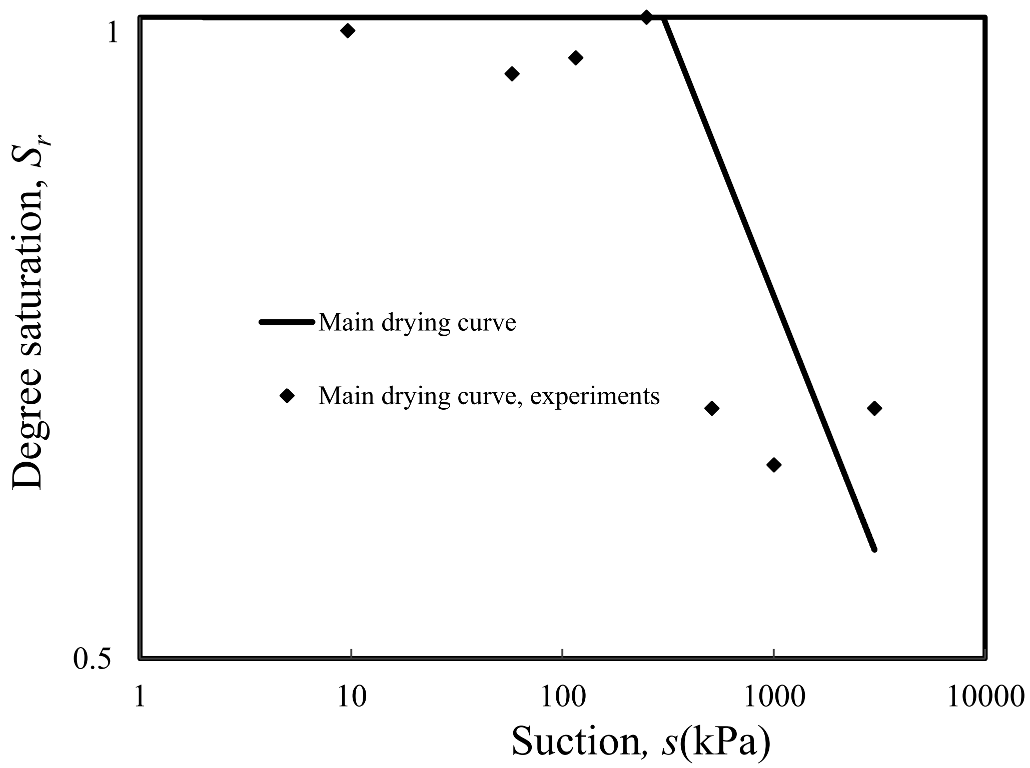

Figure 14: The behaviour of reconstituted/de-structured aggregated soil subject to drying test: The degree of saturation vs matric suction

Figures 15-18 shows the response of the aggregated unsaturated soils subject to the constant suction oedometer tests. The compression behaviour of the aggregated unsaturated soil in oedometer test during constant suction of 500 kPa is depicted in Figure 15, in terms of both net and effective stresses. It can be seen from Figure 15a that the simulated and measured responses of the compression test agree well, capturing both the shift in the yield locus due to the presence of structure and its subsequent degradation with straining. The evolution of the WRC with the applied stress is depicted in the Figure 15b. As a void ratio dependent WRC is incorporated in the numerical simulations, the model simulates satisfactorily the measured degree of saturation and its evolution during the test. Figures 16-18 compare the predicted versus measured compression response of the samples at constant suction values in the range of 1000-3000 kPa. By increasing suction, it is apparent that the strength of the soil gradually increases. The numerical simulations agree well with the experimental data for a wide range of suction values. Despite the simplicity of WRC, the water retention parameters adopted capture the necessary characteristics of experimental WRC recorded in the test. This is sufficient to record reasonable predictions. If hydraulic hysteresis is used in the simulation, the initial degree of saturation is regarded as an input parameter giving more flexibility to the WRC model. This in turn could have improved the prediction of experimental WRC. The greatest discrepancy occurs in the test with the highest suction. This is essentially due to the unreliability of the test data. This particular test reports a reduction in the degree of saturation with volumetric contraction at constant suction, which is physically unacceptable. The observed reduction in the degree of saturation is considered to be due to the lack of humidity control in the sample and hence of loss of water to evaporation during testing.

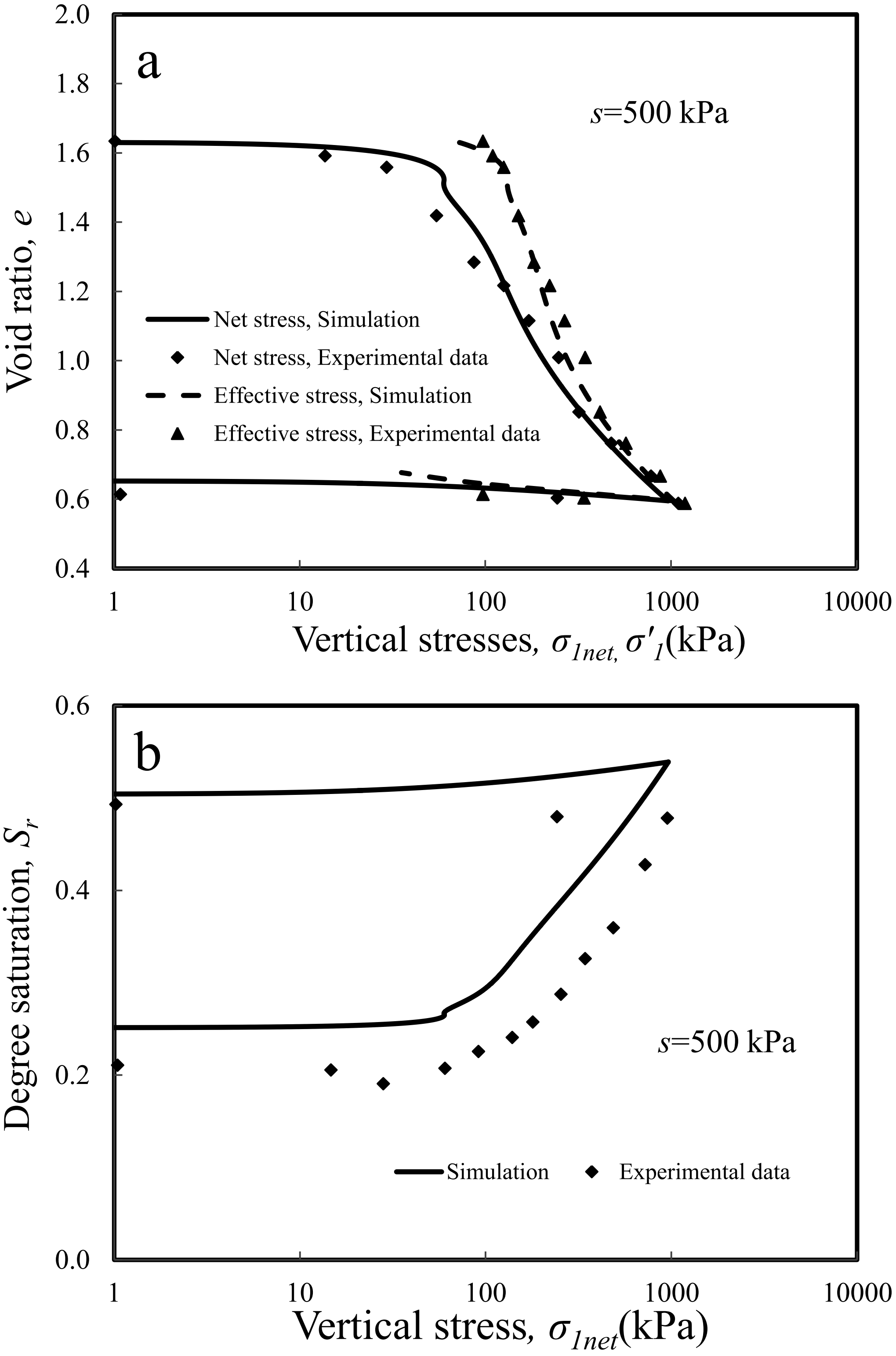

Figure 15: The oedometer response of the aggregated soil at suction 500 kPa: a) the void ratio vs. vertical net stress b) the degree of saturation vs. vertical net stress

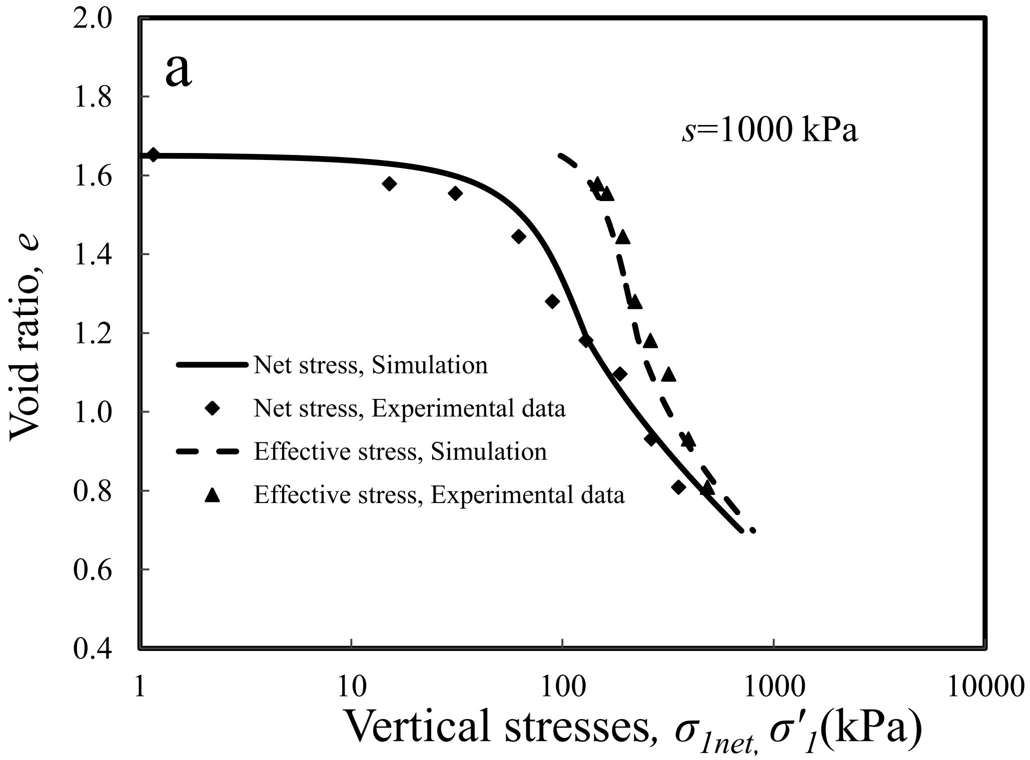

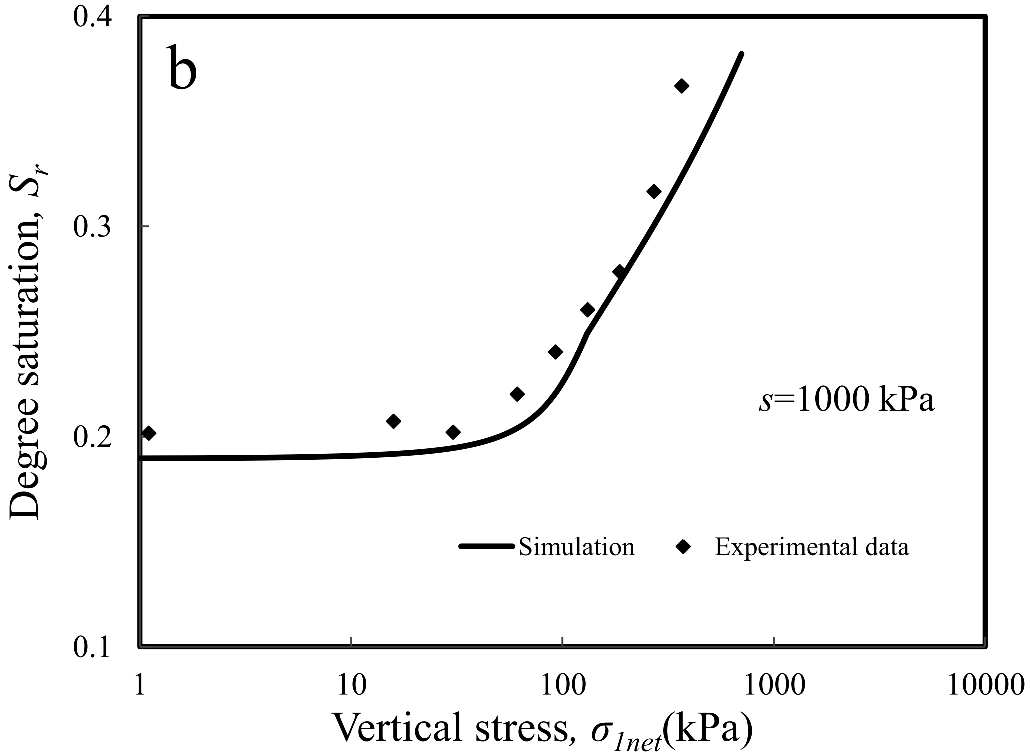

Figure 16: The oedometer response of the aggregated soil at suction 1000 kPa: a) the void ratio vs. vertical net stress b) the degree of saturation vs. vertical net stress

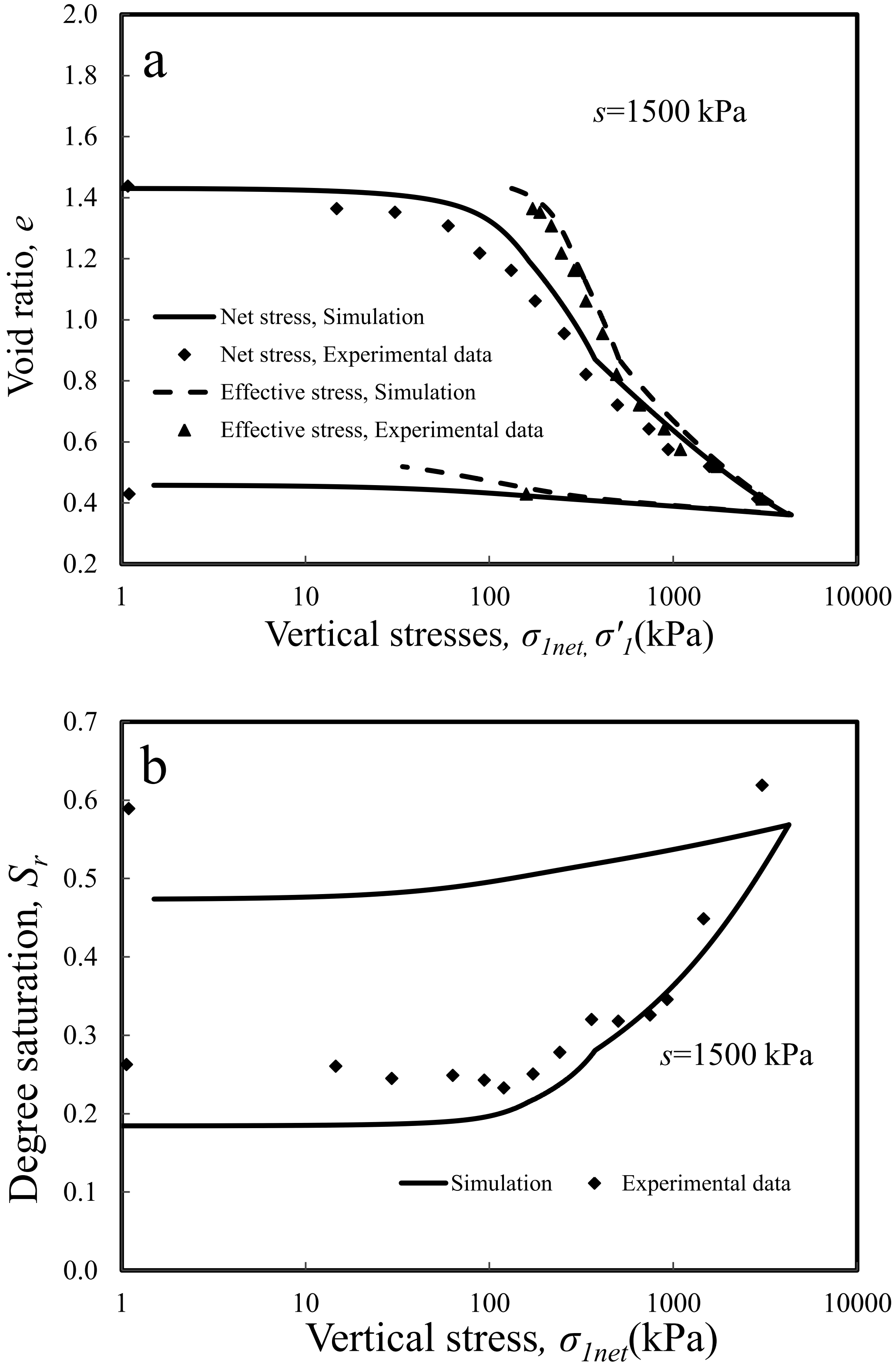

Figure 17: The oedometer response of the aggregated soil at suction 1500 kPa: a) the void ratio vs. vertical net stress b) the degree of saturation vs. vertical net stress

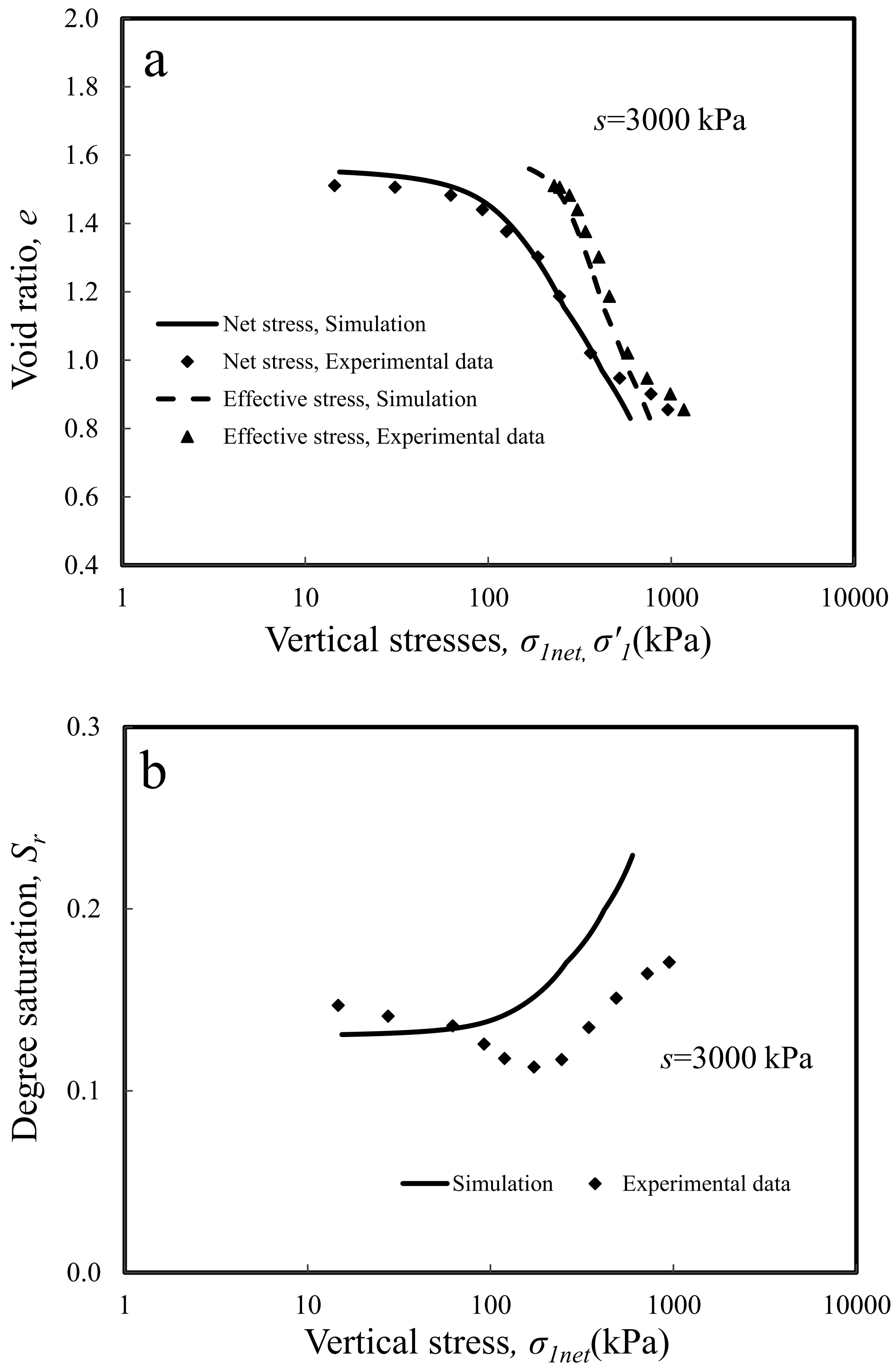

Figure 18: The oedometer response of the aggregated soil at suction 3000 kPa: a) the void ratio vs. vertical net stress b) the degree of saturation vs. vertical net stre

15. Conclusions

A bounding surface plasticity model is presented to predict the behaviour of unsaturated structured soils subjected to mechanical and hydraulic loadings. The adopted water retention model accounts for the volume change-dependency without introducing additional material parameters. A bounding surface plasticity formulation is developed, which includes the effects of hardening caused by initial structure and reduction of the degree of saturation. The degradation of the initial structure is captured through a plastic structure index rendered a function of the accumulated plastic work. This ensures that the simultaneous effects of the stress magnitude and the accumulated plastic strain can trigger the de-structure/degradation process even within the range of small deformations. The effects of tensile strength and loading path are involved in the volume change relation of structured soils. The capability of the model is investigated though simulating of laboratory tests conducted on structured soils under both saturated and unsaturated conditions. It is shown that the model can capture the key aspects of the behaviour of unsaturated structured soils.

Notations:

S_{eff}, S_r, S_{res}	Effective degree of saturation, degree of saturation and residual degree of saturation
s, p_a, p_w	Matric suction, pore air pressure and pore water pressure
χ, ψ, ψ_v	Effective stress parameter and its increment with respect to matric suction and volumetric strain
s_e	The suction value marking the transition between saturated and unsaturated state
λ_p, λ_{psu}	The pore size distribution index, its value at s_e
$\lambda_{pd}, \lambda_{pw}$	the pore size distribution indexes corresponding to the main drying and wetting curves
s_{ae}, s_{ex}	The suction values corresponding to the air entry and air expulsion
ξ, ζ	The slope of the transition line between the main drying and wetting paths in a $\ln(S_{eff}) - \ln(s)$ plane and $\ln(\chi) - \ln(s)$ plane respectively
s_r, s_{rd}, s_{rw}	The points of suction reversal, and the corresponding values on the main drying and main wetting paths
$\bar{p}'_c$	Size of the bounding surface on the hydrostatic axis
$\bar{p}'_s, \bar{p}'_m, \bar{p}'_t$	Parameters related to degree saturation strength, the compression strength of the structure and the tension strength of the structure
ρ_c	The structure degradation parameter
I_s	Structure index

p', $\bar{p}'$	Mean effective stress at the current and image points
q, $\bar{q}$	Deviatoric stress computed on the current stress points and image points
θ, $\bar{\theta}$	Lode angle of the current stress and image points
p'_c	Isotropic hardening parameter-size of the loading surface on its symmetry axis
N, R	Bounding surface shape and curvature parameters
$\mathbf{n}, \bar{\mathbf{n}}$	Normal vector of the loading/bounding surface at the current/image point
$\mathbf{m}$	Normal vector of the plastic potential at the current stress point
m_p, m_q	Volumetric and deviatoric components of the flow rule
p_0	Size of the plastic flow on the hydrostatic axis
p'_1, p'_{cs}	The reference effective mean pressure and the mean effective stress at critical state
A, k	Material parameters
$M_{cs}(\theta), M_{cs}(\bar{\theta})$	Slope of the critical state line in the plane of the current stress point and the image point
$M_{\max}, M_{\min}$	Slope of the critical state line in compression and extention
ϕ'_{cs}	critical-state internal frictional angle
d	Dilatancy
F, f, g	Surfaces for Bounding , loading and plastic potential
$\tilde{t}$	Parameter controlling the direction of plastic flow
h_b, h, h_f	Hardening moduli at $\bar{\boldsymbol{\sigma}}'$, $\boldsymbol{\sigma}'$ and an arbitrary hardening module
ξ_{cs}	State parameter
k_m, k_{mu}	Scaling parameter for the first time loading and unloading/reloading stages
ν	Poisson's ratio
$\upsilon, \upsilon_{cs}, \upsilon_{LICL}$	Specific volume at the current stress, the critical state and LICL corresponding to p'
$\lambda(1), \lambda(Sr_0)$	Slopes of the isotropic compression line in $\upsilon - ln(p')$ plane for saturated and unsaturated state
$\Gamma(1), \Gamma(Sr_0)$	Initial specific volume for the CSL at $p' = 1kPa$ for saturated and unsaturated state
$N(1), N(Sr_0)$	The intercept of the LICL at the reference pressure p'_1 for saturated and unsaturated state
κ	Slope of the unloading/reloading line in $\upsilon - \ln(p')$ plane
K, G	Elastic bulk and shear moduli

$\varepsilon_v, \varepsilon_q$	Volumetric and deviatoric strain
$\mathbf{s}, \mathbf{e}$	Tensor of devitoric stress and deviatoric strain
$\dot{\boldsymbol{\varepsilon}}, \dot{\boldsymbol{\varepsilon}}^{e}, \dot{\boldsymbol{\varepsilon}}^{p}$	Increment of strain tensor and its elastic and plastic components
$\boldsymbol{\sigma}', \boldsymbol{\sigma}'_{H}, \bar{\boldsymbol{\sigma}}'$	The current stress point, the stress at the centre of homology and the image point, respectively
$\mathbf{D}^{e}, \mathbf{D}^{ep}$	Elastic stiffness tensor, plastic elasto-plastic tensor
$\dot{\Lambda}$	Plastic multiplier
$\dot{w}^{p}, \dot{W}^{p}, \dot{E}^{p}$	The absolute rate of plastic work, total rate of plastic work and the rate of the plastic energy
$\boldsymbol{\alpha}$	the kinematic hardening vector defining the location of the loading surface
$\boldsymbol{\delta}$	Kronecker delta
α	The ratio of CSL in compression to the extension
β	The mapping rule parameter
e	Void ratio

References

ALONSO, E. E., PEREIRA, J.-M., VAUNAT, J. & OLIVELLA, S. 2010. A microstructurally based effective stress for unsaturated soils. *Géotechnique,* 60**,** 913-925.

AMOROSI, A. & RAMPELLO, S. 2007. An experimental investigation into the mechanical behaviour of a structured stiff clay. *Géotechnique,* 57**,** 153-166.

ARROYO, M., AMARAL, M., ROMERO, E. & VIANA DA FONSECA, A. 2013. Isotropic yielding of unsaturated cemented silty sand. *Canadian Geotechnical Journal,* 50**,** 807-819.

ASAOKA, A., NAKANO, M. & NODA, T. 2000. Superloading yield surface concept for highly structured soil behavior. *Soils and Foundations,* 40**,** 99-110.

BAUDET, B. & STALLEBRASS, S. 2004. A constitutive model for structured clays. *Géotechnique,* 54**,** 269-278.

BISHOP, A. W. & BLIGHT, G. 1963. Some aspects of effective stress in saturated and partly saturated soils. *Geotechnique,* 13**,** 177-197.

BORJA, R. I. 2004. Cam-Clay plasticity. Part V: A mathematical framework for three-phase deformation and strain localization analyses of partially saturated porous media. *Computer methods in applied mechanics and engineering,* 193**,** 5301-5338.

BROOKS, R. & COREY, T. 1964. HYDRAU uc Properties Of Porous Media. *Hydrology Papers, Colorado State University,* 24.

EINAV, I. & LIU, M. 2020. The Effective Stress of Unsaturated Soils: Thermodynamic Connections to Intrinsic and Measured Suctions. *Views on Microstructures in Granular Materials.* Springer.

GALLIPOLI, D., GENS, A., SHARMA, R. & VAUNAT, J. 2003. An elasto-plastic model for unsaturated soil incorporating the effects of suction and degree of saturation on mechanical behaviour. *Géotechnique.,* 53**,** 123-136.

GEORGIANNOU, V. & BURLAND, J. 2006. A laboratory study of slip surface formation in an intact natural stiff clay. *Géotechnique,* 56**,** 551-559.

HORPIBULSUK, S., LIU, M. D., LIYANAPATHIRANA, D. S. & SUEBSUK, J. 2010. Behaviour of cemented clay simulated via the theoretical framework of the structured cam clay model. *Computers and Geotechnics,* 37**,** 1-9.

HU, C. & LIU, H. 2015. A new bounding-surface plasticity model for cyclic behaviors of saturated clay. *Communications in Nonlinear Science and Numerical Simulation,* 22**,** 101-119.

KAVVADAS, M. & AMOROSI, A. 2000. A constitutive model for structured soils. *Géotechnique,* 50**,** 263-273.

KHALILI, N., HABTE, M. & ZARGARBASHI, S. 2008. A fully coupled flow deformation model for cyclic analysis of unsaturated soils including hydraulic and mechanical hystereses. *Computers and Geotechnics,* 35**,** 872-889.

KHALILI, N., HABTE, M. A. & VALLIAPPAN, S. 2005. A bounding surface plasticity model for cyclic loading of granular soils. *International Journal for Numerical Methods in Engineering,* 63**,** 1939-1960.

KHALILI, N. & KHABBAZ, M. 1998. A unique relationship of chi for the determination of the shear strength of unsaturated soils. *Geotechnique,* 48.

KHALILI, N. & ZARGARBASHI, S. 2010. Influence of hydraulic hysteresis on effective stress in unsaturated soils. *Geotechnique,* 60**,** 729.

KOHGO, Y., NAKANO, M. & MIYAZAKI, T. 1993. Theoretical aspects of constitutive modelling for unsaturated soils. *Soils and foundations,* 33**,** 49-63.

KOLIJI, A., LALOUI, L. & VULLIET, L. 2009. Behaviour of unsaturated aggregated soil in oedometric condition. *Soils and Foundations,* 49**,** 369-380.

KOLIJI, A., LALOUI, L. & VULLIET, L. 2010a. Constitutive modeling of unsaturated aggregated soils. *International Journal for Numerical and Analytical Methods in Geomechanics,* 34**,** 1846-1876.

KOLIJI, A., VULLIET, L. & LALOUI, L. 2010b. Structural characterization of unsaturated aggregated soil. *Canadian Geotechnical Journal,* 47**,** 297-311.

LALOUI, L., KLUBERTANZ, G. & VULLIET, L. 2003. Solid–liquid–air coupling in multiphase porous media. *International Journal for Numerical and Analytical Methods in Geomechanics,* 27**,** 183-206.

LEROUEIL, S. & BARBOSA, P. D. A. Combined effect of fabric, bonding and partial saturation on yielding of soils. Unsaturated soils for Asia. Proceedings of the Asian Conference on Unsaturated Soils, UNSAT-ASIA 2000, Singapore, 18-19 May, 2000, 2000. AA Balkema, 527-532.

LEROUEIL, S. & VAUGHAN, P. 1990. The general and congruent effects of structure in natural soils and weak rocks. *Géotechnique,* 40**,** 467-488.

LIU, M. & CARTER, J. 2002. A structured Cam Clay model. *Canadian Geotechnical Journal,* 39**,** 1313-1332.

LORET, B. & KHALILI, N. 2000. A three- phase model for unsaturated soils. *International journal for numerical and analytical methods in geomechanics,* 24**,** 893-927.

LORET, B. & KHALILI, N. 2002. An effective stress elastic–plastic model for unsaturated porous media. *Mechanics of Materials,* 34**,** 97-116.

MAŠÍN, D. 2010. Predicting the dependency of a degree of saturation on void ratio and suction using effective stress principle for unsaturated soils. *International Journal for Numerical and Analytical Methods in Geomechanics,* 34**,** 73-90.

MOGHADDASI, H., ESGANDANI, G. A., KHOSHGHALB, A., SHAHBODAGH-KHAN, B. & KHALILI, N. 2017. A bounding surface plasticity model for unsaturated soils accounting for the void ratio dependency of the water retention curve. *Poromechanics VI.*

MOGHADDASI, H., SHAHBODAGH, B., ESGANDANI, G., KHOSHGHALB, A. & KHALILI, N. 2021. Generalized Mapping Rule for Image Point Identification in 3D Bounding Surface Plasticity Models. *International Journal of Geomechanics,* 21**,** 04021093.

NGUYEN, L. D., FATAHI, B. & KHABBAZ, H. 2014. A constitutive model for cemented clays capturing cementation degradation. *International Journal of Plasticity,* 56**,** 1-18.

NOVA, R., CASTELLANZA, R. & TAMAGNINI, C. 2003. A constitutive model for bonded geomaterials subject to mechanical and/or chemical degradation. *International Journal for Numerical and Analytical Methods in Geomechanics,* 27**,** 705-732.

OURIA, A. 2017. Disturbed state concept–based constitutive model for structured soils. *International Journal of Geomechanics,* 17**,** 04017008.

PASHA, A. Y., KHOSHGHALB, A. & KHALILI, N. 2017. Hysteretic Model for the Evolution of Water Retention Curve with Void Ratio. *Journal of Engineering Mechanics,* 143**,** 04017030.

PEREIRA, J.-M., ROUAINIA, M. & MANZANAL, D. 2014. Combined effects of structure and partial saturation in natural soils. *Journal of Geo-Engineering Sciences,* 2**,** 3-16.

RAVEENDIRARAJ, A. 2009. *Coupling of mechanical behaviour and water retention behaviour in unsaturated soils.* University of Glasgow.

ROBIN, V., JAVADI, A. A., CUISINIER, O. & MASROURI, F. 2015. An effective constitutive model for lime treated soils. *Computers and Geotechnics,* 66**,** 189-202.

ROUAINIA, M. & MUIR WOOD, D. 2000. A kinematic hardening constitutive model for natural clays with loss of structure. *Géotechnique,* 50**,** 153-164.

ROWE, P. W. 1962. The stress-dilatancy relation for static equilibrium of an assembly of particles in contact. *Proc. R. Soc. Lond. A,* 269**,** 500-527.

RUSSELL, A. & KHALILI, N. 2006. A unified bounding surface plasticity model for unsaturated soils. *International Journal for Numerical and Analytical Methods in Geomechanics,* 30**,** 181-212.

RUSSELL, A. R. & KHALILI, N. 2004. A bounding surface plasticity model for sands exhibiting particle crushing. *Canadian Geotechnical Journal,* 41**,** 1179-1192.

SHAHBODAGH, B., HABTE, M., KHOSHGHALB, A. & KHALILI, N. 2017. A bounding surface elasto- viscoplastic constitutive model for non- isothermal cyclic analysis of asphaltic materials. *International Journal for Numerical and Analytical Methods in Geomechanics,* 41**,** 721-739.

SHAHBODAGH, B., MAC, T. N., ESGANDANI, G. A. & KHALILI, N. 2020. A Bounding Surface Viscoplasticity Model for Time-Dependent Behavior of Soils Including Primary and Tertiary Creep. *International Journal of Geomechanics,* 20**,** 04020143.

SHENG, D., SLOAN, S. & YU, H. 2000. Aspects of finite element implementation of critical state models. *Computational mechanics,* 26**,** 185-196.

SHENG, D., SMITH, D. W., W. SLOAN, S. & GENS, A. 2003. Finite element formulation and algorithms for unsaturated soils. Part II: Verification and application. *International Journal for Numerical and Analytical Methods in Geomechanics,* 27**,** 767-790.

SUN, D., SHENG, D., CUI, H. & SLOAN, S. 2007. A density- dependent elastoplastic hydro-mechanical model for unsaturated compacted soils. *International journal for numerical and analytical methods in geomechanics,* 31**,** 1257-1279.

TERZAGHI, K. V. The shearing resistance of saturated soils and the angle between the planes of shear. First international conference on soil Mechanics, 1936, 1936. 54-59.

VAN GENUCHTEN, M. T. 1980. A closed-form equation for predicting the hydraulic conductivity of unsaturated soils 1. *Soil science society of America journal,* 44**,** 892-898.

WESLEY, L. D. 1990. Influence of structure and composition on residual soils. *Journal of Geotechnical Engineering,* 116**,** 589-603.

WHEELER, S. & SIVAKUMAR, V. 1995. An elasto-plastic critical state framework for unsaturated soil. *Géotechnique,* 45**,** 35-53.

WOOD, D. M. 1990. *Soil behaviour and critical state soil mechanics*, Cambridge university press.

XIAO, J.-Q., DING, D.-X., JIANG, F.-L. & XU, G. 2010. Fatigue damage variable and evolution of rock subjected to cyclic loading. *International Journal of Rock Mechanics and Mining Sciences,* 47**,** 461-468.

YAN, W. & LI, X. 2010. A model for natural soil with bonds. *Geotechnique*.

YANG, C., CARTER, J. P., SHENG, D. & SLOAN, S. W. 2016. An isotach elastoplastic constitutive model for natural soft clays. *Computers and Geotechnics,* 77**,** 134-155.

YANG, C., CUI, Y.-J., PEREIRA, J.-M. & HUANG, M. 2008. A constitutive model for unsaturated cemented soils under cyclic loading. *Computers and Geotechnics,* 35**,** 853-859.

YASIN, S. & TATSUOKA, F. 2000. Stress history-dependent deformation characteristics of dense sand in plane strain. *Soils and Foundations,* 40**,** 77-98.

YU, H., TAN, S. & SCHNAID, F. 2007. A critical state framework for modelling bonded geomaterials. *Geomechanics and Geoengineering,* 2**,** 61-74.

YU, H. S. 1998. CASM: a unified state parameter model for clay and sand. *International Journal for Numerical and Analytical Methods in Geomechanics,* 22**,** 621-653.